Scholars' Mine

Masters Theses
Student Theses and Dissertations

Spring 2010

Quantification of channel performance and development and characterization of small magnetic field probes

Surbhi Mittal

QUANTIFICATION OF CHANNEL PERFORMANCE AND

DEVELOPMENT AND CHARACTERIZATION OF SMALL MAGNETIC FIELD

PROBES

by

SURBHI MITTAL

A THESIS

Presented to the Faculty of the Graduate School of the

MISSOURI UNIVERSITY OF SCIENCE AND TECHNOLOGY

In Partial Fulfillment of the Requirements for the Degree

MASTER OF SCIENCE IN ELECTRICAL ENGINEERING

2010

Approved by

Dr. Jun Fan, Advisor
Dr. David Pommerenke
Dr. Richard E. DuBroff
Dr. Daryl Beetner

ABSTRACT

This thesis presents a new approach to quantifying channel performance using a transmitter waveform and dispersion penalty (TWDP) with frequency domain S-parameter data. Initially TWDP was defined to characterize the performance of a transmitter in optical links. More recently its use has been extended to include the quantification of channel performance, especially in high-speed copper links. This project focused mainly on channel characterization. Instead of using the time-domain oscilloscope measurements involved in the original approach, it proposes a new method that relies on frequency-domain S-parameter data obtained either from measurements or simulations. It included a parametric study of TWDP with respect to factors such as bit rate, number of samples, and rise/fall time. This paper discusses the parameters and the results of that study.

This thesis also describes a means to obtain a flat frequency response from the first-order-derivative behavior of an electrically small loop and an electrically short electric field probe by using both in combination with active oscilloscope probes. Several magnetic field (H-field) probes based on flex-circuit technology were designed to operate at up to about 5 GHz. The H-field probe terminals were connected to the differential amplifier of the active oscilloscope probe, which functioned as an integrator to achieve a flat frequency response. The integrator behavior compensated for the first-order-derivative response of the flex circuit probes.

Another H-field probe was designed as a new approach to ensure high sensitivity without compromising spatial resolution. This thesis describes full wave simulations of the 1-mil probe and analyses the result.

ACKNOWLEDGMENTS

Words cannot adequately express my sincere gratitude to my advisor, Dr. Jun Fan, for his constant support of my work. His belief in me, his encouragement, and his guidance throughout the course of my stay in the electromagnetic compatibility laboratory are much appreciated. I would also like to thank Dr. David Pommerenke for helping me with a significant portion of my thesis. Technical discussions with him helped me better understand my subject and nurtured my curiosity. In addition, I am thankful to Dr. Richard E. DuBroff and Dr. Daryl Beetner for their encouragement of my research work, and their guidance during seminar presentations. Most importantly, I thank them for agreeing to serve on my committee. One additional member of the EMC laboratory offered significant support during my master's program; Dr. James L. Drewniak's encouragement has been invaluable.

I would also like to express my gratitude to my collaborators, Kuifeng Hu of Agilent and Xiaopeng Dong of Intel; they deserve special thanks for helping me with my research. In addition I thank fellow students at the EMC laboratory for their assistance and camaraderie: Huang Wei, Francesco De Paulis, Tun Li, ShaoHua Li, Shao Peng, and Zhang Ji. Special thanks go to Sandeep Chandra for encouraging me to join the EMC laboratory.

Finally, I would like to express my gratitude to my family for their unconditional encouragement and constant support throughout my education. I am glad to dedicate my thesis to my parents for supporting me financially and emotionally during my stay here.

TABLE OF CONTENTS

LIST OF ILLUSTRATIONS

Page

LIST OF TABLES

Page

1. INTRODUCTION

1.1. TRANSMITTER WAVEFORM AND DISPERSION PENALTY (TWDP)

Originally a transmitter waveform and dispersion penalty (TWDP) was a parameter used to quantify the performance of a transmitter. It is commonly specified and used in high-speed optical links such as 10GBASE-LRM [1-2].

A high-speed digital signal has a broad spectrum with many frequency components that travel through a transmission channel at the varying speeds. Therefore, each component reaches the receiver at a different time. This phenomenon is known as dispersion [3]. The nonlinearities in the transmitter along with a highly dispersive cable or channel can cause the link to fail because the common equalizer structures are designed for ideal channels. The TWDP test can determine whether the link will fail. It gives a measure of the losses and dispersions that occur in a transmission line/cable when a waveform travels through it.

1.2. BACKGROUND

Before the TWDP test was introduced, the transmitter and dispersion penalty (TDP) test was often specified, e.g., by the IEEE 802.3ae standard committee, to test the quality of the transmitter; however the TDP testing procedure has some drawbacks. It involves several hardware components, including a transmitter, cable, and receiver, that increase costs. Furthermore, these components can be difficult to arrange such that the results will be repeatable and consistent across multiple setups. The TWDP test, on the other hand, requires no reference transmitter, channel, or receiver; therefore, it is much simpler and less expensive. Thus is reduces the overhead involved in calibrating the reference transmitter and receiver for every setup [2].

1.3. MOTIVATION

Figure 1-1 shows the standard procedure to calculate the TWDP value. The process involves time-domain oscilloscope measurements at the output of the system under test which is a transmitter in the original TWDP application. The test uses an ideal data pattern (specified as PRBS9 in the IEEE standard). The output waveform from the system under test is captured using an oscilloscope with a fourth-order Bessel Thomson response for waveform acquisition. This output waveform is used as an input to the TWDP algorithm defined by the IEEE standard, which compares it with the ideal data pattern [1]. Both the output waveform and the ideal undistorted input waveform are fed into an emulated channel cascaded with an emulated equalizer and an emulated receiver that are both incorporated into the algorithm. To achieve the same output bit error rate (BER) at the receiver, transmitter output waveform requires a larger signal-to-noise (S/N) ratio than the ideal input waveform. The value of the TWDP is the difference in the required S/N levels for a fixed-output BER, normally 10^{-12}.

The TWDP procedure can be extended to quantify channel performance as well. In this application, the system is a physical channel (e.g., a cable) instead of a transmitter. Thus an emulated channel is not necessary in the TWDP algorithm. The output waveform and the ideal input waveform are fed directly into an emulated equalizer and an emulated receiver. The TWDP value represents the decrease in the input S/N ratio when the physical channel is replaced with an ideal lossless channel while keeping the output BER the same for both channels. This application of TWDP application has already been used to characterize high-speed copper links such as the 10 Gb/s SFP+ copper link [4-5].
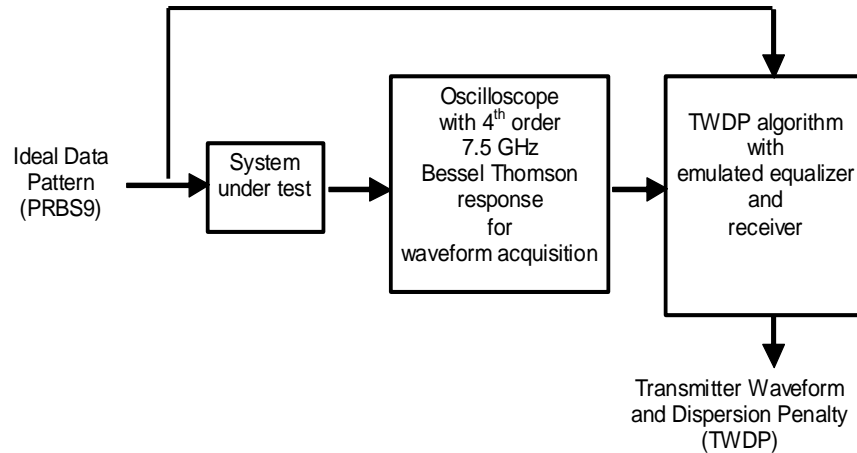
Figure 1-1: Conventional TWDP measurement procedure

Physical channels are often band limited with loss. Further, the transmission loss of a channel usually increases with frequency. For example, both conductor and dielectric losses exist in a copper cable. The high-frequency conductor loss (i.e., the skin-effect loss) is proportional to the square root of the frequency, whereas the dielectric loss increases in proportion to frequency. This frequency-dependent loss in a channel is a major factor in the distortion of digital signals as they pass through the channel. Another important factor is the phase of the channel transfer function. If this phase is not linear, the channel can result in dispersion in the output signal.

The TWDP parameter quantifies the effects of the transfer function of a channel on high-speed digital signal transmission. It is related to inter-symbol interference (ISI) but is more intuitive because it is a quantifiable. The higher the TWDP value is, the more distortion in the output waveform of the channel. In other words, the channel becomes less desirable for a high speed link.

This project focused on channel characterization using the TWDP parameter. A new method is introduced below to calculate the TWDP value associated with a physical channel based on its frequency-domain S-parameter data. A description follows of a parametric study on the effects of some factors that could be easily modified using the new approach.

1.4. FREQUENCY-DOMAIN APPROACH

As shown in Figure 1-1: Conventional TWDP measurement procedure, the conventional approach to the calculation of the TWDP value involves a time-domain oscilloscope measurement. Figure 1-2 illustrates a new approach that starts with the channel's frequency-domain S-parameters, which can be obtained from a vector network analyzer (VNA) measurement or even through numerical modeling. The S-parameters, combined with an emulated input signal having a specified data pattern, generates the time-domain output waveform through a link path analysis. This output waveform is then compared with the ideal input waveform in the TWDP algorithm, and the TWDP value is calculated.

Figure 1-3 is a flow chart of the link path analysis. A time-domain input waveform is first generated with a specified data pattern. Many parameters of this input waveform can be defined and adjusted, including bit rate, rise/fall time, high/low voltage levels, number of samples per bit, and number of bit pattern repetitions. The time-domain input waveform is then transformed into the frequency domain through the Fast Fourier Transform. The frequency-domain S-parameter data of the channel under test must also be input for the link path analysis. To obtain meaningful results, however, the data must be preprocessed before to ensure that they are physical.

And it needs to be ensured that any minor measurement errors are corrected. Both passivity and causality of the data are checked and enforced [6].
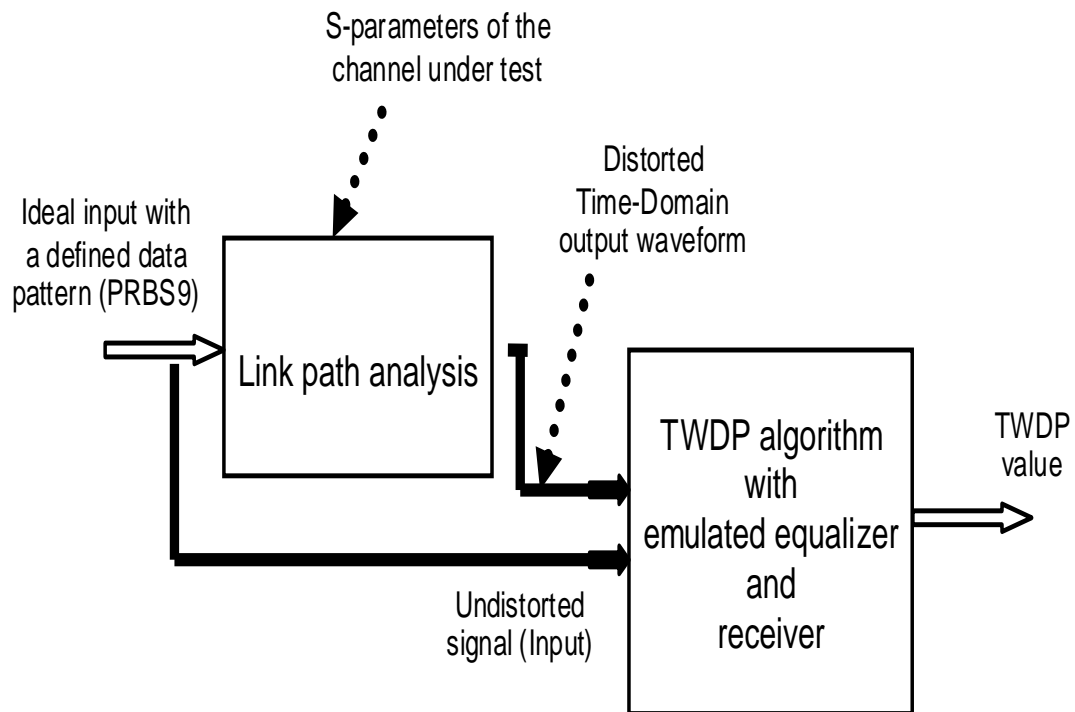
Figure 1-2: New approach to calculate the TWDP value of the channel under test.

The S-parameter data must normally be extrapolated to DC and interpolated at a preferred frequency sampling rate to ensure an accurate and meaningful inverse Fourier transform later on.

After preprocessing, the frequency-domain S-parameter data are multiplied with the frequency-domain input, resulting in the frequency-domain output of the channel. Inverse fourier transform is then employed to obtain the time-domain output waveform.
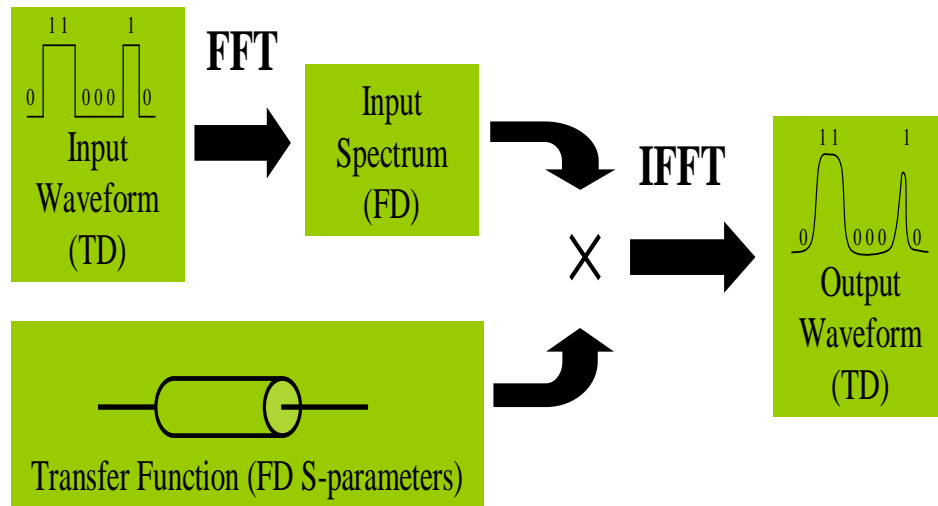
Figure 1-3: Link path analysis.

The TWDP value is calculated by comparing the time-domain output waveform with the ideal time-domain input waveform. This comparison requires an alignment of the two signals. In other words, the delay in the output waveform caused by the channel must be removed so that corresponding bits in the input and output waveforms can be aligned.

The advantages of the new TWDP approach over the conventional procedure are due in part to the elimination of the time-domain oscilloscope measurement. In the new approach, the frequency-domain S-parameters can be obtained from a VNA measurement or numerical modeling. Frequency-domain VNA measurements are much more repeatable than time-domain oscilloscope measurements. Further the VNAs have a much larger dynamic range; therefore, they can accurately capture signals both smaller and larger than those captures by oscilloscopes. Further, VNA measurements facilitate test

fixture calibration and compensation so that the effects of the test fixtures, (e.g., testing cables, connectors, adapters) can be eliminated, resulting in more accurate and reliable data.

In addition, the conventional approach requires a pattern generator to obtain an input waveform. This pattern generator is unnecessary in the new frequency-domain approach because the input waveform is emulated instead. This modification greatly reduces the cost and complexity of the measurement setup.

Finally, the results yielded by the conventional approach are affected by the properties of pattern generator and sampling scope. The same channels (cables) may yield slightly different results when tested in different labs with different equipments. No such inconsistency occurs with S-parameters, which change little when measured on different systems with proper handling and calibration.

The new approach offers some tangential benefits as well. Almost all the parameters can be freely changed to study various hypothetical scenarios. For example, the data rate is no longer limited to 10.3125 GHz; nor is the number of samples per bit to 16. In addition to PRBS9, any data patterns are allowed. Thus the user has a great deal of freedom in the design of various test setups. These advantages make the new approach a useful tool for evaluating the TWDP parameter, and it will facilitate future improvements and adjustments.

1.5. RESULTS AND DISCUSSION

This approach used the new approach to conduct a parametric study of the TWDP with respect to setup parameters such as data rate, number of samples per bit, rise/fall time, and number of pattern repetitions. The TWDP values were plotted as a function of a

setup parameter. The channel tested here was a 6-meter 24AWG SFP+ copper cable including two differential pairs.

Figure 1-4 shows the TWDP value of one differential pair as a function of the data rate. As expected, the TWDP value increased with frequency. The frequency spectrum of a higher-speed digital signal had more high-frequency components, whereas the loss in the copper cable increased significantly with frequency. Thus, more distortion was caused by the channel to the higher-speed digital signal, resulting in a larger TWDP value. The figure further indicates that the relationship between the TWDP value and the data rate was approximately linear. Therefore it may be possible to estimate the TWDP value for a cable at a given frequency, provided that the TWDP values at a certain set of frequencies have already been determined.
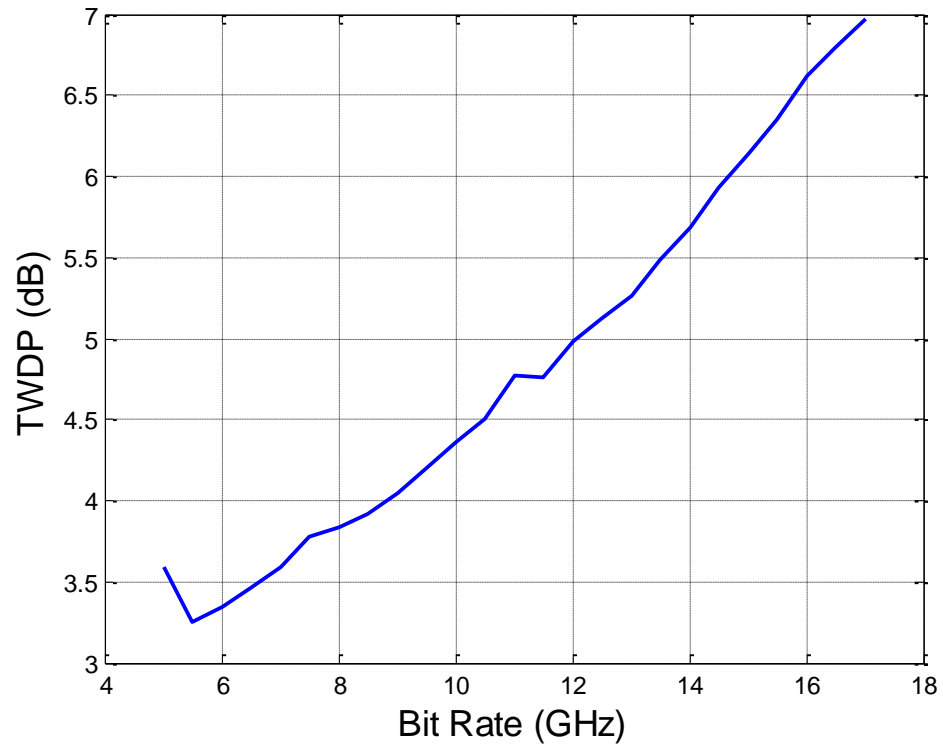
Figure 1-4: TWDP versus bit rate.

Figure 1-5 shows the variation in TWDP value with respect to the number of samples per bit. It clearly indicates that the 16 samples per bit specified by the current standard may be insufficient. The TWDP values began to converge when the number of samples per bit was larger than 40. Increasing this sampling rate can result in a more accurate TWDP value.
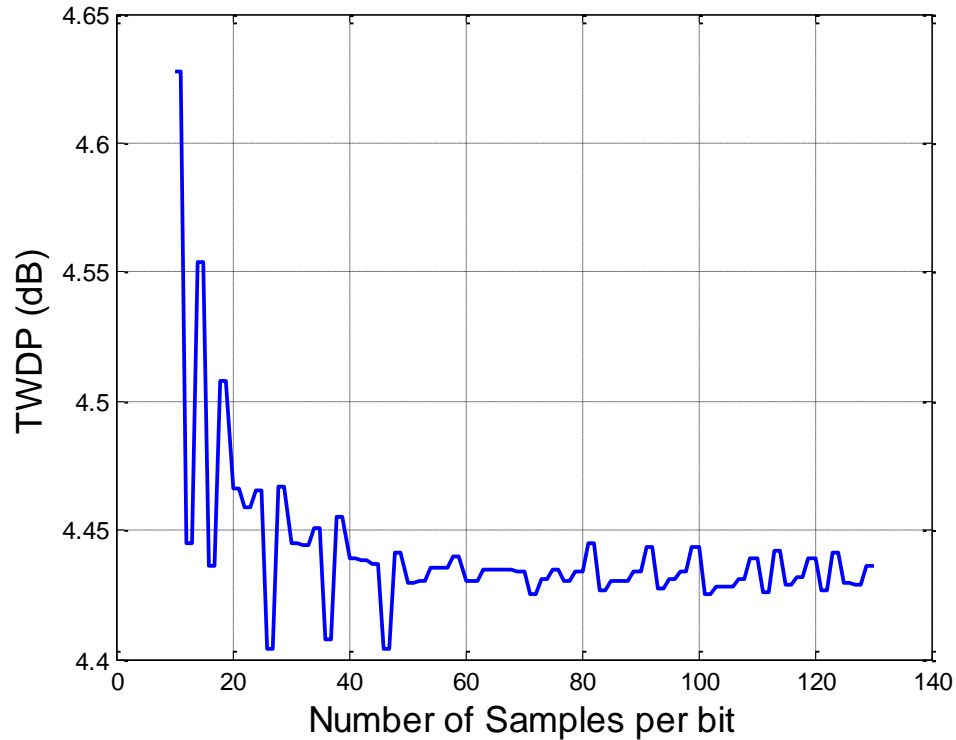
Figure 1-5: TWDP versus number of samples per bit.

The TWDP value also changed with the rise/fall time, as illustrated in Figure 1-6. The data rate in this case was fixed at 10.3125 GHz, and the rise/fall time varied within the allowable range. Generally, the TWDP value decreased with the increase in rise/fall time. This effect is explained by the fact that the shorter rise/fall time cause more higher-frequency components in the signal spectrum. Because the channel adds more loss at higher frequencies, the signal with a shorter rise/fall time is distorted more after it passes through the channel. The relationship is not linear; rather, it has many step shapes, a characteristic that demands further investigation.
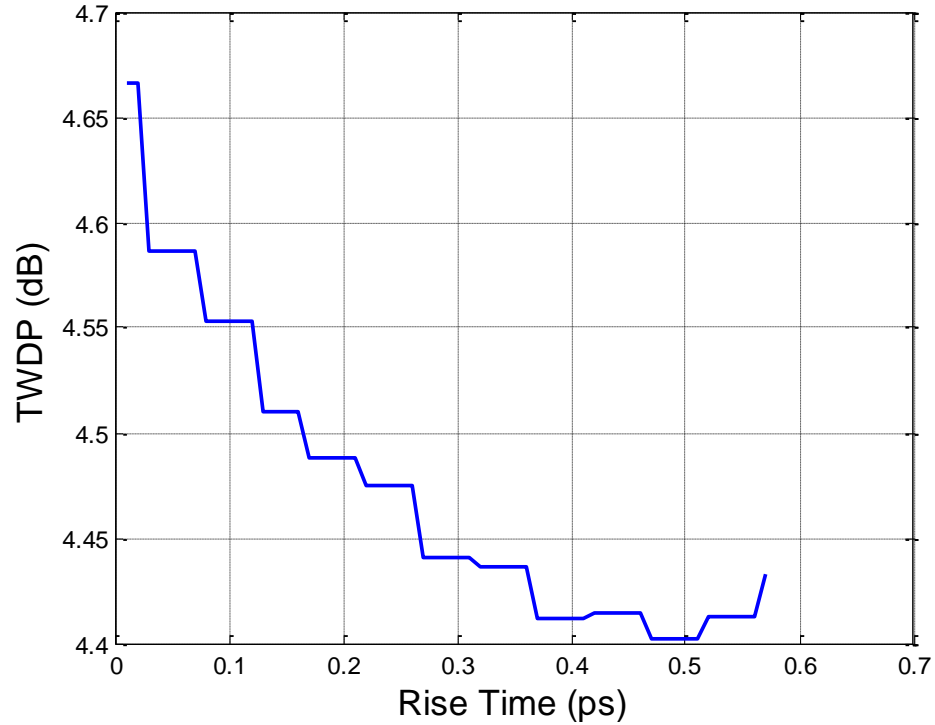
Figure 1-6: TWDP versus rise/fall time.

Figure 1-7 shows the TWDP value as a function of the number of pattern repetitions. The number of pattern repetitions is the number of times the input waveform pattern is repeated; therefore, this factor determines the length of the input data stream. The TWDP value decreased slightly as the number of pattern repetitions increased, perhaps due to a transient response when the input waveform began. The TWDP value changed little with increase in repetitions from 1 to 9. It is alright to use 1 repetition for simulation to save simulation time.
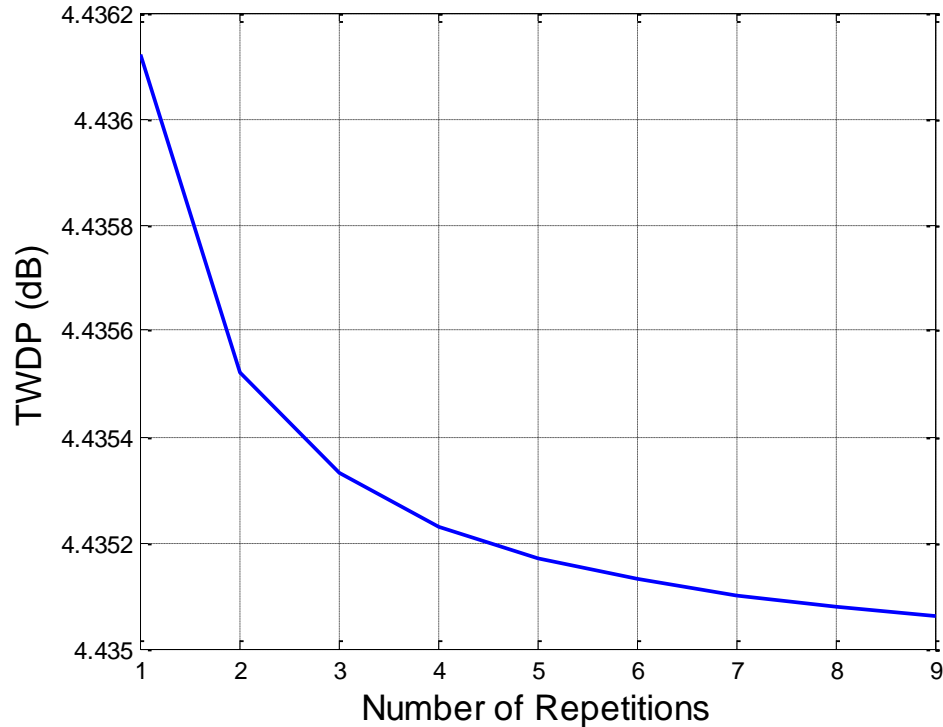
Figure 1-7: TWDP versus number of pattern repetitions.

1.6. TWDP BASED ON SAS SPECIFICATIONS

This report presents the results of simulation test results performed on a couple of S-parameter files using the TWDP calculator developed at electromagnetic compatibility laboratory (EMC Lab) in Missouri University of Science and Technology. The S-parameter files were obtained by measuring six channels on a backplane. All the files were single ended measurements with 1 & 3 as input and 2 & 4 as output ports.

The simulations were performed at a data rate of 6 GB/s with 20% to 80% of transition. For convergence, 100 samples were used per bit. Rise/Fall times were varied in the allowable range of 41.6 ps to 67 ps. Pseudo random bit sequence 9 (PRBS9) was

applied because PRBS7 pattern changes every time it is generated in Matlab; changing the TWDP value each time even when other settings remain constant. De-emphasis of 0 dB, 2 dB and 3 dB were required; however, since the de-emphasis feature was not available, pre-emphasis was used instead. Pre-emphasis of 0 dB, 2 dB, and 3 dB were applied. This TWDP tool allows the pre-emphasis feature; however the initial bits must be enhanced to avoid bit error. The effect of both should be the same. In de-emphasis the toward the end of the series bits are lowered; thereby enhancing the initial bits.

A random jitter (RJ) of 1.47 ps (with a maximum of 0.15UI) was applied. Each channel had six different combinations of simulations for each rise/fall time.

As indicated in Table 1-1: Results of simulation of six channels at 6 GB/s the TWDP value expresses in decibels decreased as expected with an increase in pre-emphasis. The TWDP value increased with application of RJ as expected; however, in some cases there was no increase despite low variation. These cases may have been an effect of reduced convergence due to the application of fewer samples per bit. With an increase in rise time, the TWDP value also increased. Shorter rise time signals had more energy initially; thus, most of the signal reached the other end, leading to lower TWDP.

The channel with flex had the highest TWDP value of all cases. Based on the phase plot of channel SAS2, it was the longest differential pair.

Table 1-1: Results of simulation of six channels at 6 GB/s

6 Gb/sec; 100 samples per bit; PRBS9; 20-80%								
Rise Time	Pre-emphasis	Random Jitter	Without Flex	With Flex	02_Pri	10_Pri	12_Pri	SAS2
0.416 To 0.429	0 dB	0	4.47349	6.1700	2.4872	2.9532	2.8158	4.5964
		1.47 ps	4.4809	6.165	2.4988	3.006	2.8603	4.6027
	2 dB	0	3.8847	5.7789	2.077	2.5703	2.4981	4.0388
		1.47 ps	3.8852	5.7835	2.1936	2.6047	2.5127	4.21737
	3 dB	0	3.6937	5.563	1.8502	2.3758	2.4331	4.0728
		1.47 ps	3.7037	5.6475	1.8827	2.4862	2.462	4.070
0.43 To 0.449	0 dB	0	4.5124	6.1808	2.5206	2.9666	2.8486	4.6344
		1.47 ps	4.52	6.181	2.5256	3.0344	2.9344	4.664
	2 dB	0	3.8981	5.7894	2.1055	2.587	2.5196	4.0535
		1.47 ps	3.9279	5.8154	2.1113	2.6712	2.5429	4.0841
	3 dB	0	3.7007	5.5741	1.881	2.3941	2.429	4.0704
		1.47 ps	3.7356	5.6347	1.9048	2.4443	2.4643	4.3182
0.45 To 0.469	0 dB	0	4.5536	6.1922	2.555	2.98	2.889	4.6733
		1.47 ps	4.4831	6.2135	2.551	3.0272	2.951	4.65
	2 dB	0	3.9121	5.800	2.1279	2.604	2.5414	4.07
		1.47 ps	3.9847	5.8364	2.1722	2.717	2.535	4.1223
	3 dB	0	3.71499	5.5856	1.907	2.413	2.4266	4.0692
		1.47 ps	3.8978	5.5915	1.9095	2.4512	2.4568	4.1685
0.47 To 0.489	0 dB	0	4.5945	6.2031	2.5937	2.996	2.932	4.7132
		1.47 ps	4.6064	6.244	2.6151	3.1712	2.967	4.655
	2 dB	0	3.9254	5.8131	2.1505	2.6215	2.5636	4.088
		1.47 ps	4.0215	5.829	2.1695	2.6878	2.6714	4.1377
	3 dB	0	3.7307	5.5977	1.933	2.4325	2.429	4.0685
		1.47 ps	3.8836	5.6611	2.0377	2.4774	2.439	4.0807
0.49 To 0.509	0 dB	0	4.6378	6.2158	2.6338	3.0124	2.9723	4.754
		1.47 ps	4.6537	6.243	2.6474	3.0924	2.9728	4.696
	2 dB	0	3.94	5.8252	2.1792	2.6395	2.586	4.10731
		1.47 ps	4.104	5.9491	2.1976	2.6346	2.606	4.16
	3 dB	0	3.7498	5.6104	1.965	2.453	2.445	4.0685
		1.47 ps	3.782	5.6287	1.988	2.525	2.467	4.119
0.51 To 0.529	0 dB	0	4.6807	6.2292	2.6798	3.0314	3.0183	4.7958
		1.47 ps	4.911	6.3067	2.6614	3.053	2.942	4.8333
	2 dB	0	3.9554	5.839	2.2022	2.658	2.609	4.1273
		1.47 ps	3.97	5.8663	2.259	2.738	2.6194	4.1666
	3 dB	0	3.769	5.6247	1.991	2.4739	2.468	4.0694
		1.47 ps	3.7704	5.5853	2.017	2.5684	2.448	4.0908
0.53 To 0.55	0 dB	0	4.7245	6.2424	2.7227	3.055	3.0604	4.8386
		1.47 ps	4.7317	6.3056	2.7114	3.1411	3.017	4.8457
	2 dB	0	3.9722	5.8522	2.2255	2.6773	2.633	4.1479
		1.47 ps	4.197	5.8843	2.2363	2.6834	2.449	4.2300
	3 dB	0	3.7906	5.6396	2.0184	2.495	2.4944	4.0716
		1.47 ps	3.87423	5.7065	2.0465	2.615	2.599	4.0915
0.551 To 0.57	0 dB	0	4.7678	6.2579	2.767	3.086	3.1086	4.8819
		1.47 ps	4.7959	6.3079	2.73	3.1745	3.055	4.9107
	2 dB	0	3.988	5.867	2.2488	2.698	2.656	4.1691
		1.47 ps	4.0815	5.88	2.2738	2.794	2.7435	4.2395
	3 dB	0	3.8101	5.6551	2.051	2.5183	2.5206	4.0763
		1.47 ps	3.8577	5.6973	2.1017	2.6689	2.516	4.0916

Table 1-1 (continued)

0.571 To 0.589	0 dB	0	4.8120	6.2748	2.8177	3.1215	3.147	4.9266
		1.47 ps	4.7809	6.2905	2.803	3.222	3.151	4.89
	2 dB	0	4.0062	5.8826	2.2779	2.7184	2.68	4.1908
		1.47 ps	4.0411	6.048	2.3324	2.7794	2.7528	4.304
	3 dB	0	3.8321	5.6702	2.0783	2.5425	2.5473	4.0848
		1.47 ps	4.0051	5.6804	2.1187	2.6944	2.558	4.096
0.59 To 0.609	0 dB	0	4.8554	6.2925	2.865	3.1642	3.1917	4.9722
		1.47 ps	4.8689	6.3161	2.8033	3.2191	3.11	4.968
	2 dB	0	4.021	5.8976	2.30161	2.7407	2.7041	4.213
		1.47 ps	4.043	5.9572	2.3746	2.8651	2.7215	4.2676
	3 dB	0	3.853	5.6869	2.1058	2.5673	2.5744	4.0984
		1.47 ps	3.9387	5.688	2.1098	2.684	2.625	4.1155
0.61 To 0.629	0 dB	0	4.8981	6.3135	2.9139	3.204	3.226	5.019
		1.47 ps	4.85	6.3194	2.9005	3.2815	3.266	5.010
	2 dB	0	4.0395	5.914	2.325	2.763	2.729	4.2355
		1.47 ps	4.038	5.9233	2.348	2.7715	2.727	4.3331
	3 dB	0	3.8742	5.7045	2.1337	2.5926	2.6018	4.117
		1.47 ps	3.8985	5.7402	2.1563	2.6018	2.61	4.1543
0.63 To 0.649	0 dB	0	4.9437	6.337	2.964	3.2491	3.2844	5.0661
		1.47 ps	4.9021	6.3424	2.98	3.3929	3.318	5.02
	2 dB	0	4.0563	5.9314	2.3545	2.7866	2.755	4.2587
		1.47 ps	4.1222	5.9591	2.3512	2.8683	2.75	4.2723
	3 dB	0	3.8961	5.7223	2.1668	2.6226	2.6296	4.1398
		1.47 ps	3.9574	5.729	2.2113	2.7039	2.6375	4.2158
0.65 To 0.669	0 dB	0	4.9924	6.3642	3.022	3.2944	3.2901	5.1148
		1.47 ps	4.9915	6.4654	3.0208	3.278	3.293	5.10
	2 dB	0	4.0735	5.9492	2.3784	2.8135	2.7835	4.282
		1.47 ps	4.079	6.056	2.4019	2.9502	2.881	4.3579
	3 dB	0	3.9165	5.74	2.195	2.653	2.657	4.1647
		1.47 ps	4.0138	5.7916	2.2099	2.789	2.662	4.2265
0.67	0 dB	0	5.0425	6.3954	3.0757	3.2714	3.336	5.1645
		1.47 ps	5.0535	6.37455	3.0789	3.3111	3.32	5.1718
	2 dB	0	4.0898	5.967	2.4024	2.8422	2.818	4.3056
		1.47 ps	4.2993	5.968	2.418	2.9443	2.8088	4.3716
	3 dB	0	3.9352	5.761	2.2232	2.6786	2.6854	4.1912
		1.47 ps	4.0737	5.9307	2.228	2.679	2.7037	4.3167

2. FLEX CIRCUIT H-FIELD PROBES AND E-FIELD PROBE

2.1. INTRODUCTION

With the rapid development of high-frequency digital circuits, radio frequency interference (RFI) and electromagnetic compatibility/electromagnetic interference (EMC/EMI) problems are becoming more relevant in new system/circuits design and application and need to be addressed to develop improved circuits and devices [7]. The frequency spectrum of high-speed digital signals has high-frequency components [8] that interfere with the system's internal circuitry, causing unwanted radiation. The high-frequency noise is caused by the sharp edges of the digital waveforms [9]. Switching currents in integrated circuits (ICs) cause signal integrity issues and EMI compliance failures that underscore the need to develop high spatial resolution probes for pinpointing the surface currents [11-10]. Concerns are growing over self interference within systems, digital ICs, or switched power supplies, all of which disturb radio frequency (RF) receivers. Numerical computational techniques are widely used to predict such problems, but they fail when modeling is too complex [8]. The electromagnetic (EM) field mapping technique is beneficial for optimization of RF circuits and prediction of complicated EMI/EMC problems. Thus, a probe is needed to measure electric-field (E-field) or magnetic-field (H-field). This work built and characterized the flex-circuit H-field probes and dipole E-field probe. The flex-circuit H-field probes have a first order derivative frequency response; when combined with the amplifier of the 1169A Agilent active probe, it gives a flat frequency response. The E-field probe represents an extended application of the Agilent active probe to give a flat frequency response. To produce a flat frequency response, it requires high impedance loading that can be achieved by using

an active probe. This report describes the development and characterization of these high-resolution H- and E-field probes.

The flex circuit H-field probes were developed to function as stand-alone and in combination with existing active probe (i.e., the Agilent 1169A active probe). Due to their small loop sizes, they are less sensitive, but their sensitivity could be improved by either of two methods. First, probes could be designed with larger loop sizes. This modification would increase mutual inductance between the probe and the PCB trace, thereby increasing the sensitivity of the probe. A variety of such probes can be created. Second, the number of turns could be increased. Multiplied magnetic flux would cause much higher mutual inductance thus increasing the sensitivity. The three-turn flex-circuit probes described here have been designed but not yet manufactured due to costs.

Both approaches increase self-inductance

$$V_{out} = j\omega I_{trace} \cdot M \cdot \frac{Z_{load}}{j\omega L_{self} + Z_{load}} \qquad (1)$$

where M is the mutual inductance between the current on the trace and the H-field loop; I_{trace} is the current on the trace; Z_{load} is the impedance of the loading terminal of the H-field (e.g., the input impedance of the oscilloscope or network analyzer (NWA)); and L_{self} is the self-inductance of the loop.

Figure 2-1 demonstrates that self-integration frequency is lower when the loop has higher self inductance. Two loop sizes were chosen for this simulation, one with self-inductance of 0.5 nH and the other with self inductance of 2 nH. The latter showed self integration at lower frequencies with increased sensitivity, and the former self-integrates at higher frequencies.
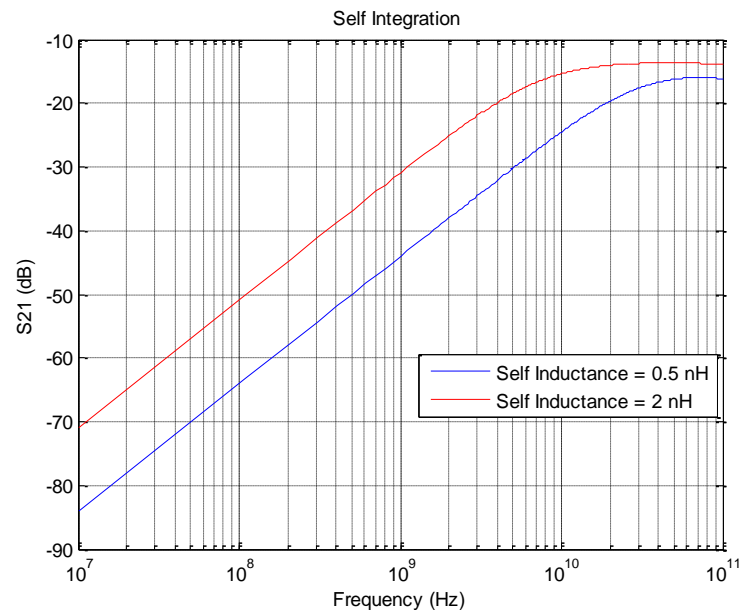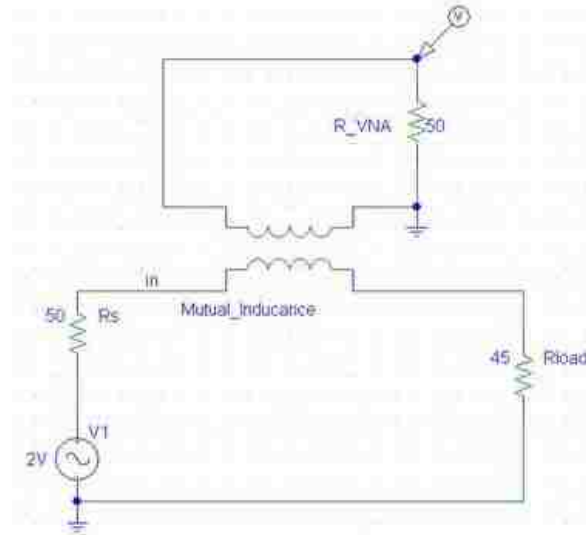
Figure 2-1: PSPICE model and simulation result of self integration frequency

Over the frequency range in which the effect of self-inductance is negligible, the frequency response of the H-field loop probe rises at 20dB/dec. This property can be offset by attaching an active probe with an amplifier (as described in Chapter 3). As shown in Figure 2-1, if the self-inductance is increased to achieving higher sensitivity, the frequency range in which this measure works is limited.

This work designed and tested a model of an E-field probe. The model was found to possess a sensitivity of 3.3 mV/(V/m). (The procedure used to calculate sensitivity is detailed in Appendix C). Due to its size, this probe disturbs the E-field more than do magnetic field probes. The probe could be downsized, but this would reduce its sensitivity. From a measurement point of view, it is convenient to create probes with matching sensitivities:

$$E_{Sensitivity}/_{377} = H_{Sensitivity} \tag{2}$$

where $E_{sensitivity}$ is the sensitivity of E-field probe; and $H_{sensitivity}$ is the sensitivity of the H-field probe and 377 Ω is the intrinsic impedance of atmosphere.

This report describes an approach to obtain a flat frequency response from electrical (or magnetic) field probes by using them in combination with active probes. It also introduces the H-field differential probes designed to operate at higher frequencies (on the order of gigahertz) and built using flex-circuit technology. An E-field probe was designed and developed based on a bow tie antenna design. This Thesis introduces a new method to obtain a flat frequency response from B-dot and D-dot field probes by attaching them to active oscilloscope probes, which are available in most labs. Active

probe amplifiers can be used as both E and H-field probes to achieve a reasonably wide band flat frequency response.

This Thesis also introduces first-order derivative H-field probes based on flex-circuit technology. These probes can operate at up to a few gigahertz, and they have a high spatial resolution.

Flex circuit technology facilitates the design of smaller probes than those developed using PCB technology without complicating their connection with connectors. Thin film technology allows even finer probes, but these require more complex transitions to coaxial connectors.

The following section also discusses an E-field probe designed by extending the application of the active probe.

2.2. BACKGROUND

Electromagnetic (EM)-field mapping has proved beneficial not only to optimize and adjust RF circuits but also to predict complicated EMI/EMC problems. Problems of growing concern include self-interference within systems, digital ICs, or switched power supplies, all of which disturb RF receivers. Various kinds of magnetic field (B-dot/H-dot) sensors are commercially available, and numerous articles have addressed probes [7]-[14]. These sensors show a first-order derivative frequency response (FR). To recover the EM field waveform from data captured by these sensors, analog or numerical integration is required. Such integration is difficult to achieve over a many-decade bandwidth because the dynamic range of the data captured by the oscilloscope is limited. To overcome this problem several non differentiating sensors have been developed based on transverse electromagnetic (TEM) horn, resistively loaded dipoles, or dipoles with curved

arms [9].These sensors, however, are large. Yarovoy, de Jhang and Ligthart [10] have describes a free space sensor based on a shielded-loop antenna with a reasonably flat FR.

2.3. ACHIEVEMENTS

The flex-circuit H-field probes are designed to be used in the gigahertz frequency range. When combined with the differential amplifier of the 1169A active probe, they give a flat frequency response. By implementing some de convolution code on the scope to improve the low frequency and by using a de-embedding procedure to remove the effects of probe loading, a flat frequency can be expected over a band of roughly 10 MHz to 3 GHz.

2.4. FLEX CIRCUIT H-FIELD PROBES

2.4.1. The Design. Flex-circuit H-field probes have trace width of the order of 1.75 mils. A variety of flex probes have been built and the smallest loop has a size of 3x3 mils. These small probes are suitable for magnetic field scanning on lead frames of ICs or highly dense PCBs, e.g., flex circuits connecting different PCBs. The larger probes offer greater sensitivity but lower resolution. The self-resonance frequency of these probes is on the order of tens of gigahertz.

The flex circuit probe is a differential H-field probe. Figure 2-2 shows its basic design. The probe's loop dimensions are '5x5 mils'. The probe is electrically shielded on all sides and has two plated slots at the tip of the loop. The slots ensure that the coupled magnetic field can normally generate the induced voltage on the loop, and the metal shield successfully prevents the coupling of the electrical field. It has ground (GND) vias located on all its boundaries, ensuring good electrical shielding. The gap at the tip of the probe is made in order to break the continuity in the loop formed by two ground planes to

prevent eddy losses. Five H-field probes have been built: their loop dimensions are 3×3 mil, 5×5 mil, 5×5 mil with T slot, 7×5 mil and 8×8 mil respectively. Appendix A shows the layout of two of these probes. A variety of via sizes were used; the smallest was 2 mils in diameter. Potential electric field coupling from the trace directly into the probe is through the 2-mil gap between the two slots. This coupling is negligible given the width of the gap.
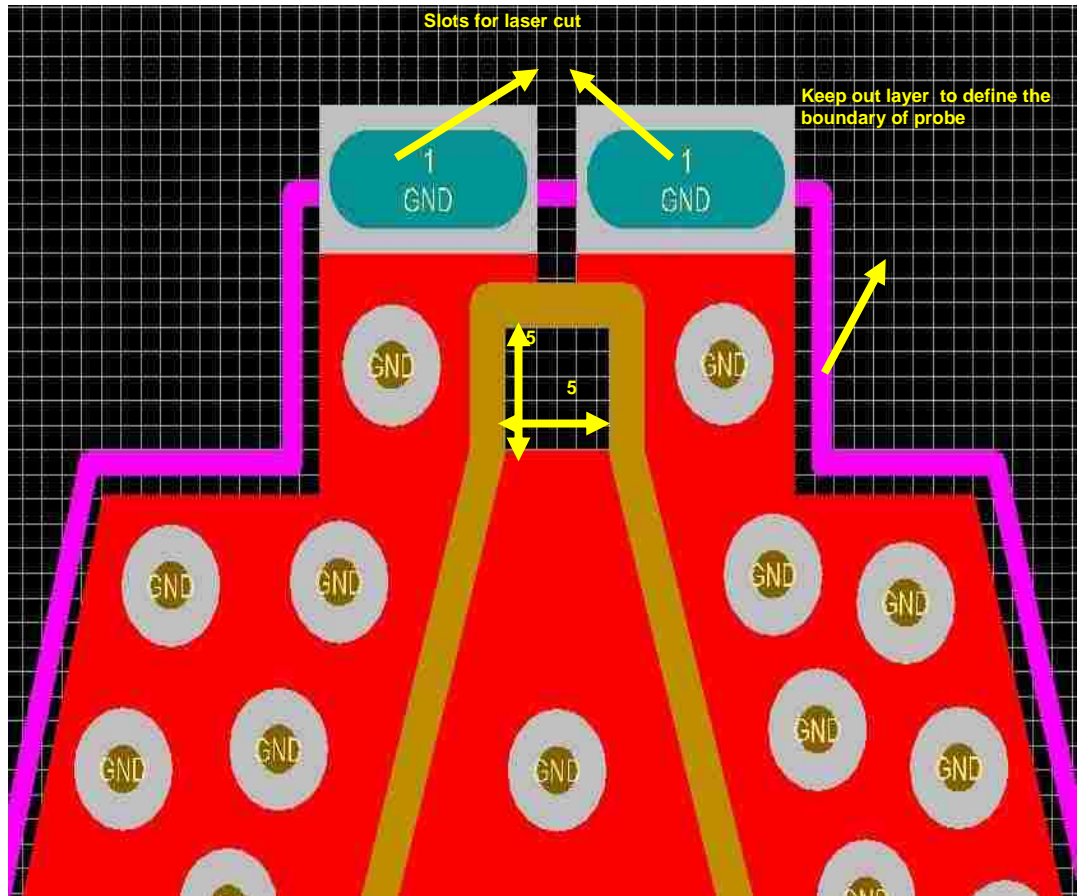

Figure 2-2: Basic Design of Flex Circuit Probe

2.4.2. Probe Development And Circuit Topology Analysis. The mini-SMP was mounted to the flex probe using a solder, and the geometry created by the mounting caused inductive and capacitive effects that were observed on the time domain Reflectometer (TDR). The excess inductance was due to the poor connection of the GND of the mini-SMP, as shown in Figure 2-3 (b) below. A gap between the solder pads of the probe and the connector causes a discontinuity that shows up as inductance in the TDR response. This gap could be fixed by clipping a portion of each connector to shorten it. Figure 2-3(c) shows a photograph of the 5 mil by 5 mil probe after the excess was clipped. The connection is smooth, and the gap is reduced to making the excess inductance negligible. The response was observed on the TDR while mounting the connector on the probe. An optimal position was found at which the effect of parasitic inductance was negligible. The dip due to excess capacitance remained, and it was found to be a property of the probe itself. The reason for this dip is explained in greater detail below. Shown below in Figure 2-3 (b) and Figure 2-3 (c) are snapshots of the probes before and after improvement and also the TDR response and PSPICE simulations compared.

Figure 2-3(a) shows the TDR response of probes before and after clipping of the mini-SMP connectors. The red curve shows the effects of both inductive and capacitive parasitics. The red circle in Figure 2-3(b) highlights the significant gap between the connectors and solder pads of the probe; this gap introduces the excess inductive effect. TDR results of the improved probe showed only the capacitive coupling. The gap between the pad on the top layer (connecting the middle layer through a blind via) and the bottom GND layer accounts for the capacitive behavior.
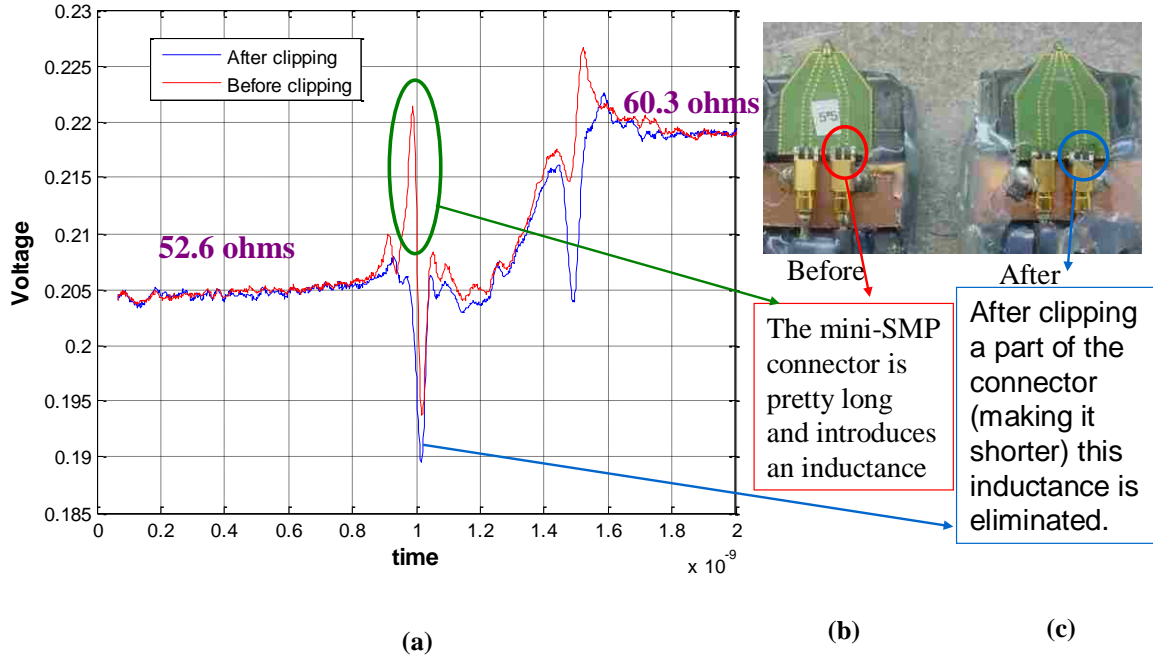
Figure 2-3: (a) TDR response of probes before and after improvement; (b) snapshot of 5mil by 5mil probe before improvement; (c) snapshot of 5mil by 5mil probe after improvement.

The value of capacitance can be calculated using the parallel plate approximation:

$$C_{p-p} = \varepsilon \times A \Big/ d \tag{3}$$

where C_{p-p} is the parallel plate capacitance; ε is the permittivity of the dielectric; A is the area of the parallel plate; and d is the separation between the plates.

Dimensions of the top pad connected to middle layer through the blind via are:

$$A = \left(0.53e^{-3}\right) \times \left(0.92e^{-3}\right) \tag{4}$$

$$d = 25 + 2 + 25 + 35 = 87 \ \mu m$$

$$C_{p-p} = 8.85e^{-12} \times 3.1 \times A \Big/ 87e^{-6} = 150 \ fF$$

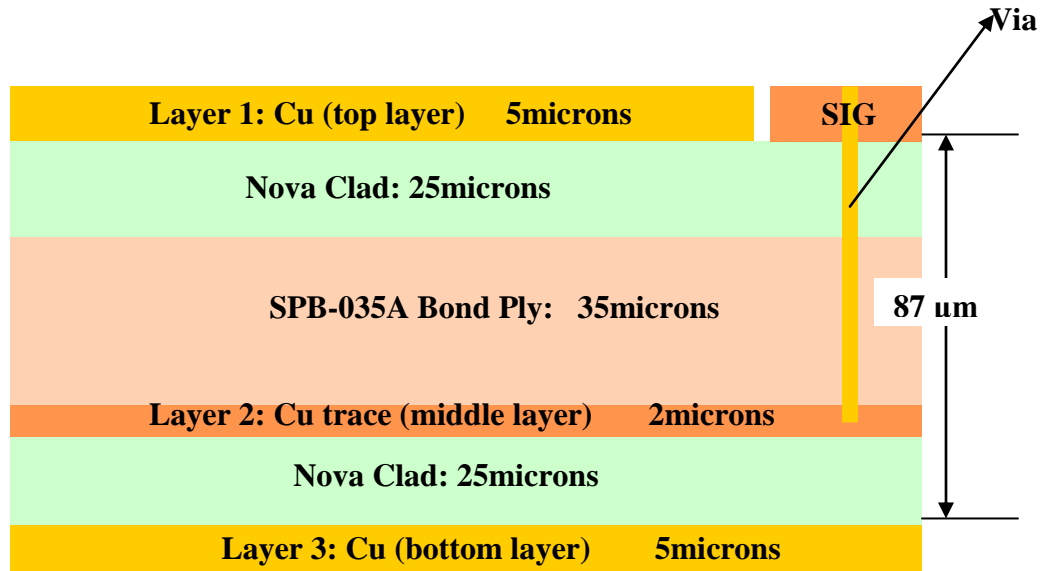Value of excess capacitance calculated from TDR = 100 fF

Figure 2-4: Cross-sectional layout of the flex circuit probe

Excess capacitance is between this pad area and
the reference ground plane i.e. bottom layer.
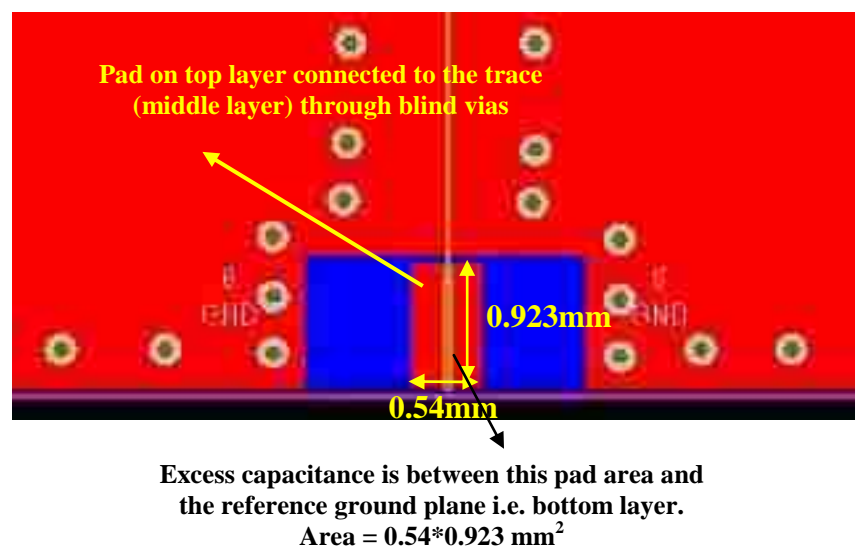Area = 0.54*0.923 mm^2

Figure 2-5: Layout of bottom part of the flex probes showing the solder pad on top layer

2.4.3. Pspice Simulation Of Probe To See Tdr And S21 Response. This work sought to determine the best probe response given an ideal trace for testing. It also sought to identify which unwanted effect in the probe (e.g. capacitance, inductance, SMA mount, resistance, etc.) has the greatest impact to understand how we would improve the design if we re-design the probe. Parasitic capacitance was calculated using TDR. Two markers were used, one at each end of transition, and the value of capacitance was found to be 100fF. This value was used in the PSPICE simulation. The schematic and results are shown in Figure 2-6 and Figure 2-7 respectively. The TDR response simulated and compared it with the actual TDR response to validate the parasitic parameters.

The network analyzer response simulation was performed by varying the values of parasitic capacitance. This capacitance was between the pad on the top layer connected to the trace through a blind via and the bottom GND-layer flex-circuit probe. This simulation determined the best response possible with the present parasitics and identified the parasitics that had the greatest impact. This information would be used to redesign the probe. The existing parasitics were:

- 100 pH excess inductance between the SMA and semi-rigid coaxial cable
- 100 fF excess capacitance due to mini-SMP mounting on the probe
- 37 Ω trace running along the probe. The probe was designed for this value of characteristic impedance of trace in the probe; however, as explained in sub-section 2.4.3.2 below, the value of Zo was not 37 Ω rather it was around 50 Ω.

2.4.3.1 Geometry Simulated In Pspice. Figure 2-6 shows the PSPICE schematic of the 5×5 mil flex circuit H-field probe. The traces within the probe were represented by 50 Ω transmission lines (Tx lines) with a time delay of 125 ps each. The loop of the probe was represented by an inductance of 0.0408 nH. These circuit values were found using time domain Reflectometer (TDR) measurements
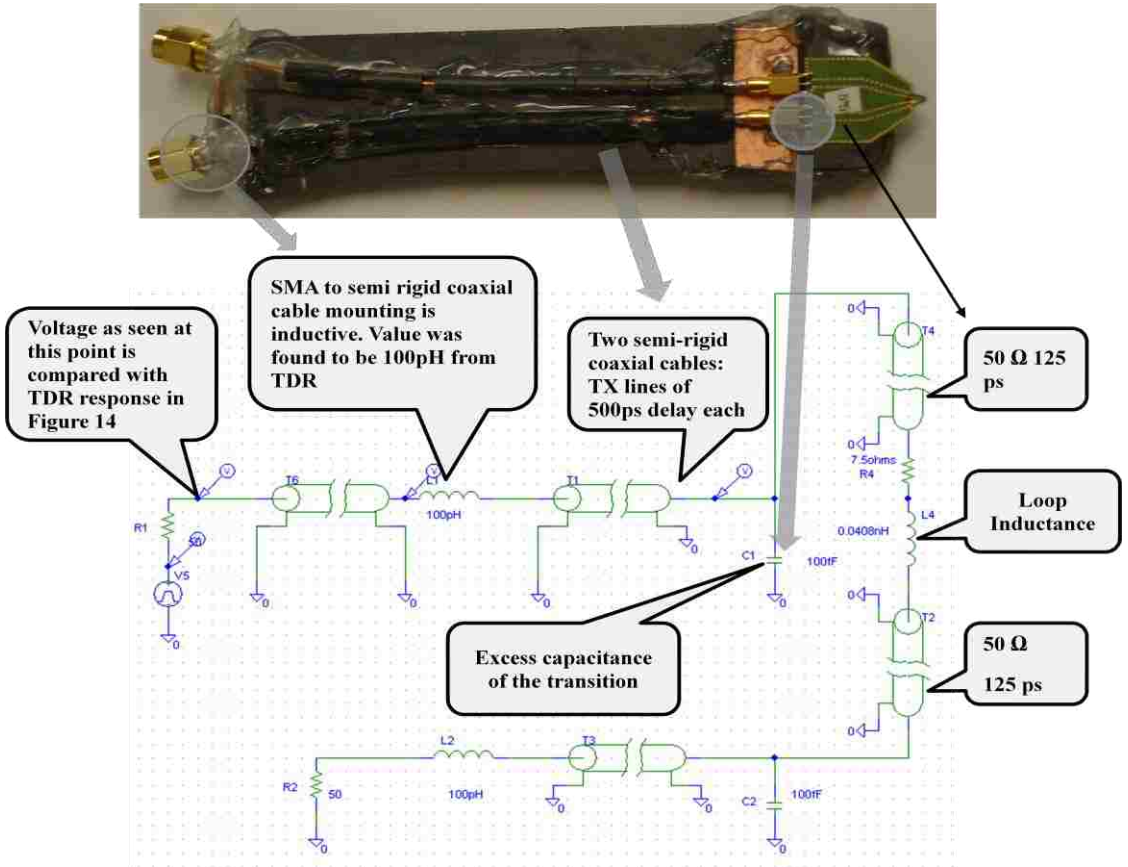

Figure 2-6: PSPICE Schematic of Probe

2.4.3.2 Tdr Response Of Improved Probe And Pspice Simulation Compared. The green curve in Figure 2-7 above shows the PSPICE simulation of the probe using the values of parasitics determined by TDR. The simulation used a 50 Ω lossless TX line. From the TDR response, the characteristic impedance of the trace of the probe was found to be around 50 Ω because immediately after the capacitive behavior at 1.1ns, the curve rose again back to around 50 Ω and remained at that level till 1.25 ns. However, the characteristic impedance for which the probes were designed was around 37 Ω which reveals a discrepancy. Also, the probe resistance as calculated from the design was around 2.2 Ω, but the actual DC resistance of the probe was calculated to be 7.5 Ω.
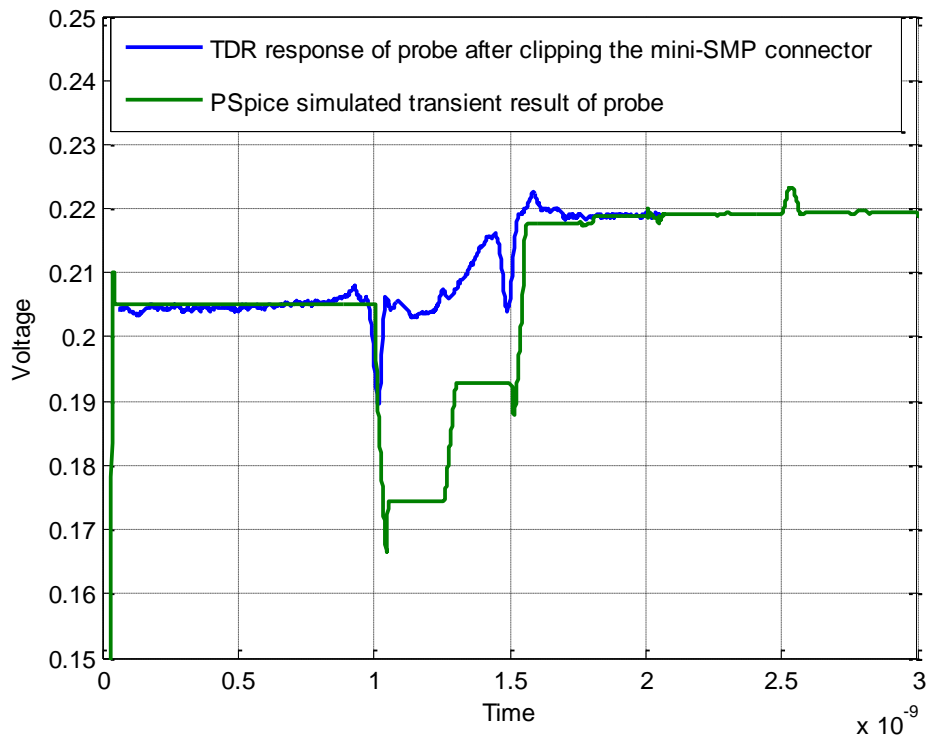

Figure 2-7: Comparison of TDR response and PSPICE simulation of 5×5 mil flex probe

Therefore, a second simulation was run for characteristic impedance of trace within probe of 50 Ω, as shown in Figure 2-8. Figure 2-9 shows the PSPICE schematic. The result of this simulation shows a closer agreement with the measured TDR response of the probe. The parasitic capacitance seemed slightly greater than the measured level.
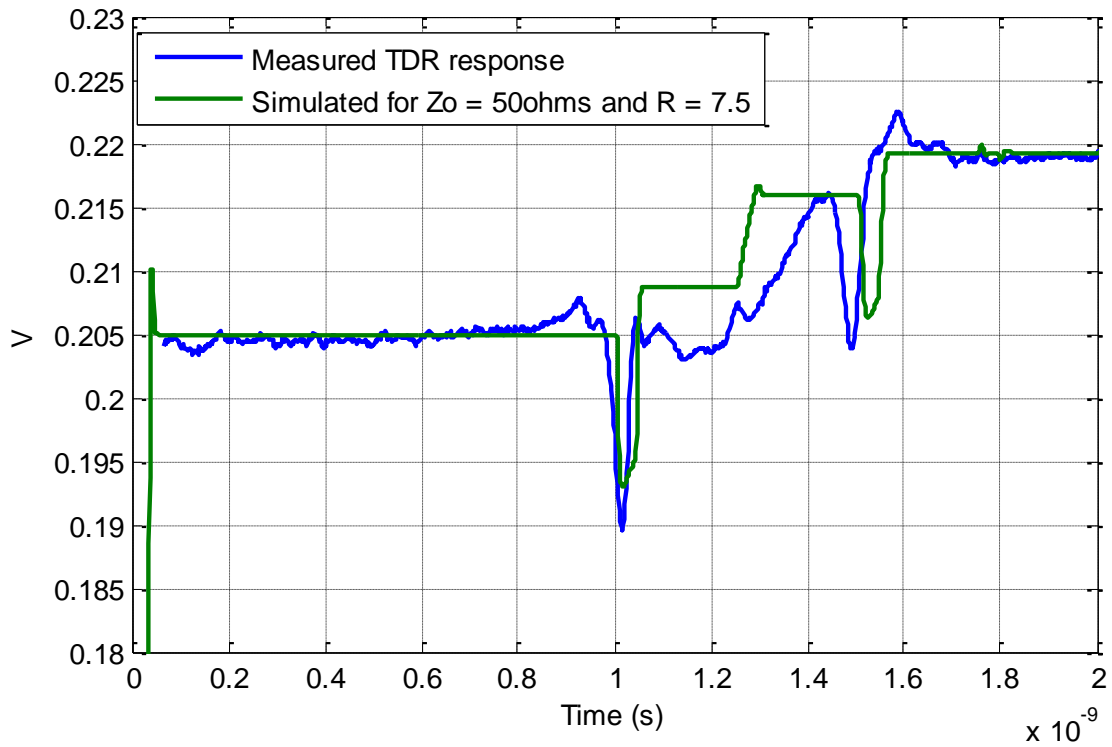

Figure 2-8: TDR response and PSPICE simulation of 5×5 mil flex probe with Zo of trace = 50 Ω

2.4.3.3 PSPICE Simulation For S21 From One Port Of The Probe To The Other. Figure 2-9 shows the PSPICE schematic of the 5×5 mil flex probe with a voltage monitor at one end of the differential probe terminated in 50 Ω load. This is used to measure the insertion loss of the probe.
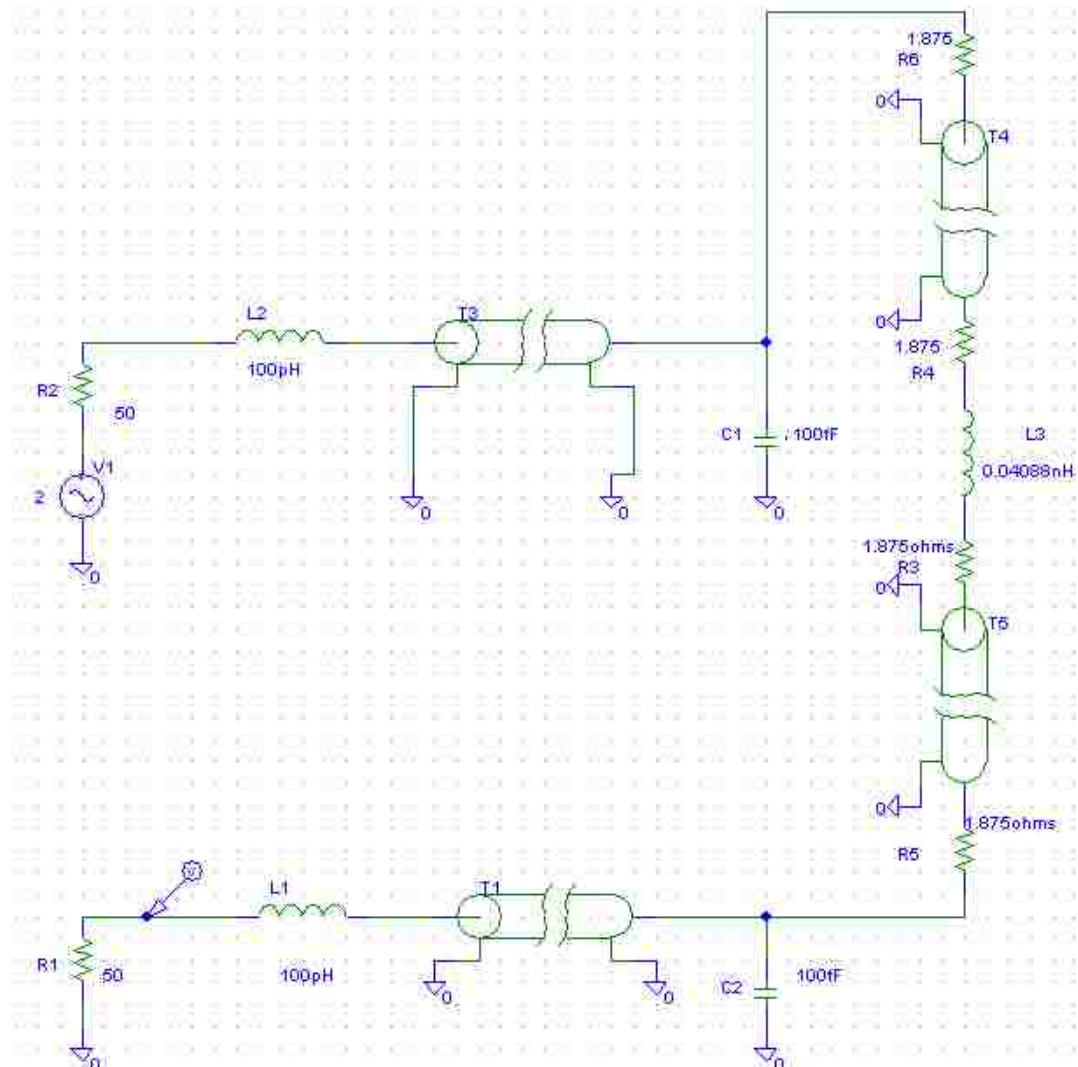

Figure 2-9: PSPICE schematic for S21 of 5×5 mil probe from one port to the other
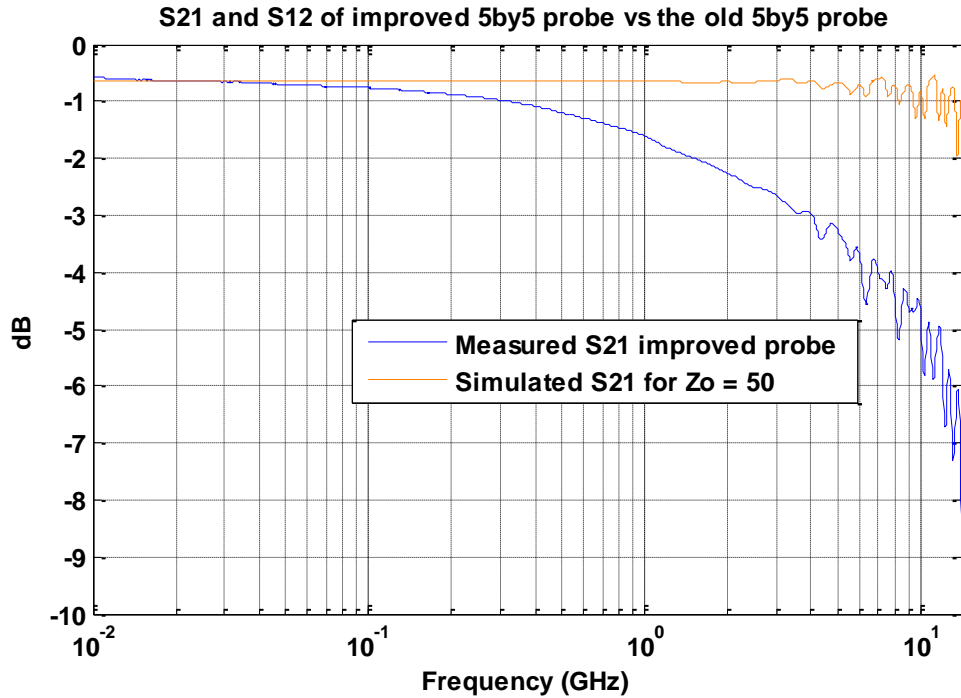
Figure 2-10: Measured and simulated S21 from one port of the 5×5 mil flex probe to the other

Figure 2-10 shows the S21 from one port of the 5 mil by 5 mil probe to the other. It compares measured and simulated results. This graph validates the existing parasitics in the flex-circuit probe. The blue curve is the measured result, and the orange curve is the simulation result. As demonstrated by the measured result, the insertion loss was -6 dB at 10 GHz. In the case of the simulation, the semi-rigid coaxial cable and the trace running in the probe were both assumed to be lossless ideal 50 Ω transmission lines, which is not the case in reality. Thus there was a difference at higher frequencies. Dielectric loss increased proportionally with frequency as shown by the measured data. These losses were significant at higher frequencies. The parasitics taken into

consideration for the simulation as in Figure 2-9 above are the excess 100 fF capacitance of the probe, the 100 pH inductance between the SMA and semi-rigid coaxial cable and the 50 Ω characteristic impedance of the trace within the probe. The losses of the probe and the semi-rigid cables attached to it were not considered in the PSPICE simulation. This plot shaped expectations for the FD response of the probe-PCB coupling. A deviation from the ideal 20 dB per decade rise was now expected. The behavior of probes when coupled with trace is discussed in the section 2.4.6.
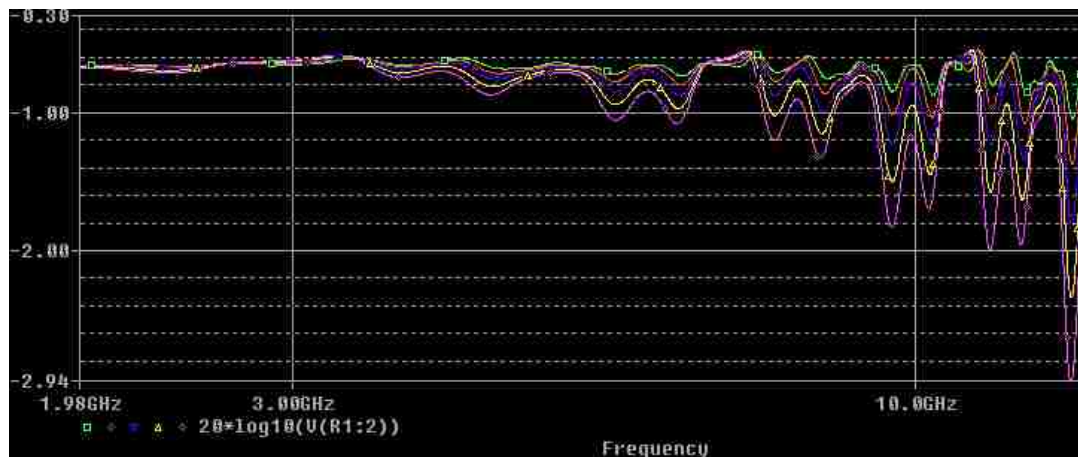

Figure 2-11: S21 for C1=C2= 30 fF to 150 fF in intervals of 30 fF

The graph in Figure 2-11 above was plotted to reveal the difference in the S21 from one port of the probe to the other when the parasitic capacitance values (C1 and C2 in the figure) were varied from 30 fF to 150 fF in steps of 30 fF. It indicates which parasitic capacitance value causes the greatest deviation from ideal behavior, permitting

effective redesign of the probes. The green trace is for parasitic C1=C2=30 fF, and the pink trace is for C1=C2=150 fF. Variation between C1 and C2 caused slight variation in S21 from one port of probe to the other at frequencies above 2GHz. Many reflections were visible at higher frequencies. The difference in insertion loss S21 for a parasitic capacitance of 30 fF and 150 fF was about 2 dB at about 13.9 GHz, a difference that would significantly affect the frequency domain (F.D) response when probe is coupled with a PCB trace. For lower parasitic capacitance, overall loss (including dielectric and conduction loss) in the probe at higher frequencies would be lower creating less deviation of the FD response from the ideal 20 dB per decade rise.

2.4.4. Pcb Trace Improvement. The PCB trace used for testing gave a flat frequency response only up to about 4GHz. Flex probes can work well up to much higher frequencies. Therefore, the PCB trace was changed. The new trace had to be cut short to fit the test setup. One end of the trace was terminated with two 90 Ω resistors in parallel as shown in Figure 2-12 below. The trace was thus made single ended.
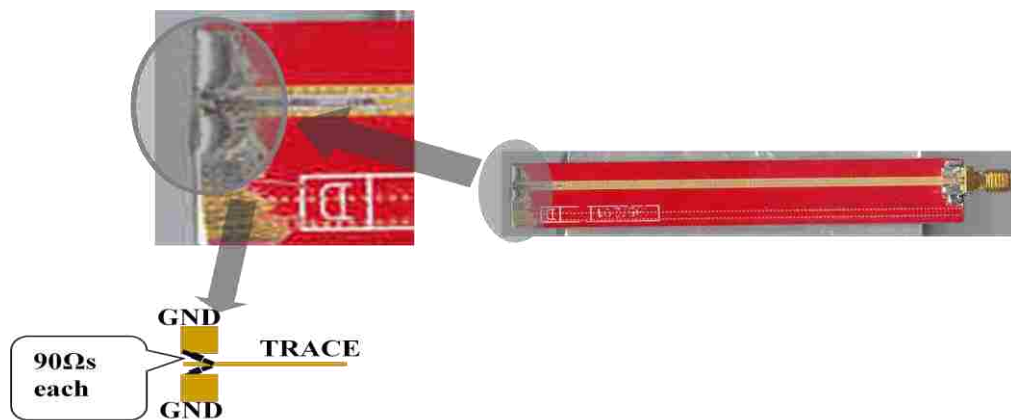

Figure 2-12: New trace from Agilent

The network analyzer response (S11) of the trace is shown in Figure 2-13.As can be seen from the response of the trace in Figure 2-13, the highest peak in S11 occurred at 15 GHz, which is equal to -15.6 dB. All other peaks at other frequencies were below this magnitude. The lower the S11, the better.

Terminating one end of the trace by 45 Ω rather than using the conventional 50 Ω termination led to lower reflections and thus a good S11 response. Reflections are lower if the transmission line is matched. Therefore, the characteristic impedance (Zo) of the trace was around 45 Ω.
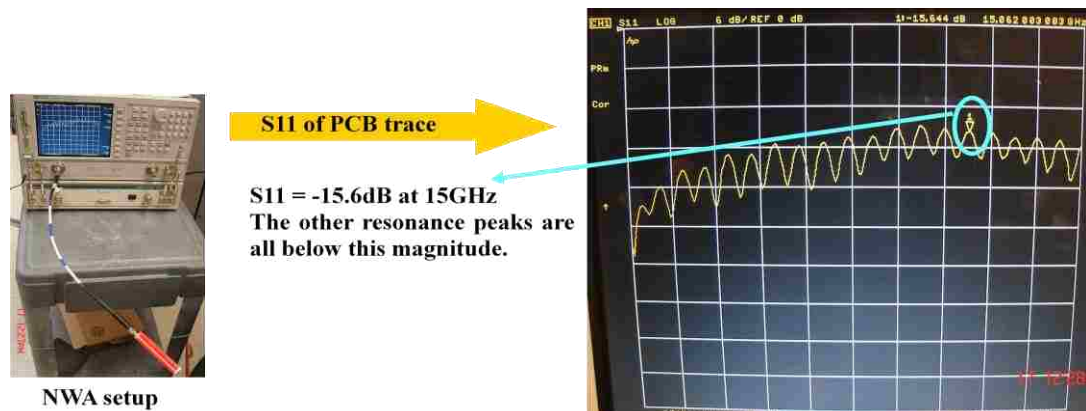

Figure 2-13: Network analyzer response of the new PCB trace from Agilent

2.4.5. Sensitivity. Sensitivity of a probe can be defined as the ability of a probe to detect field. A good first order guess of the sensitivity of the probe is its area:

$$V_{induced} = A \times \frac{\partial B}{\partial t} \tag{4}$$

where A represents the equivalent area of probe; $V_{induced}$ is the voltage induced in the probe; and *dB/dt* is the time rate of change of magnetic field.

A probe with a larger loop area can couple more energy and thus induce higher voltage than a probe with a smaller loop. A probe with a larger loop size is, therefore, better than a probe with a smaller loop. To calculate sensitivity using TEM cell method, a slot was milled through a PCB, and was placed on the 10cm^2 slot on the top wall of the TEM cell as shown in Figure 2-14. The probe was then held in the slot with its loop perpendicular to the fields inside the TEM cell. The S21 response of the coupling between the fields inside the TEM cell and the probe was measured using the vector network analyzer (VNA). Voltage could then be determined analytically from S21. An effective loop area was determined to describe the sensitivity within the region in which the frequency response follows a first order derivative function. Figure 2-15 illustrates the fields inside the Crawford TEM cell and the coupling between the cell and the flex probe when it is placed inside the TEM cell.
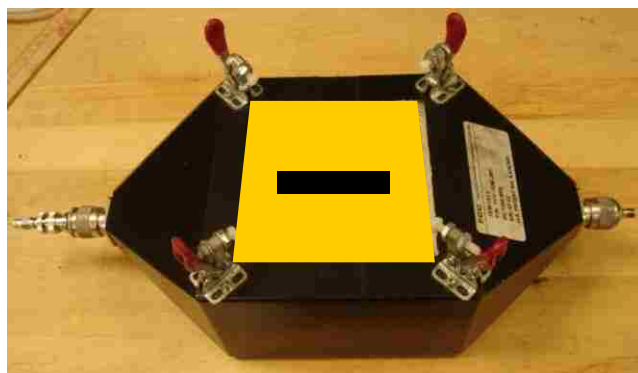

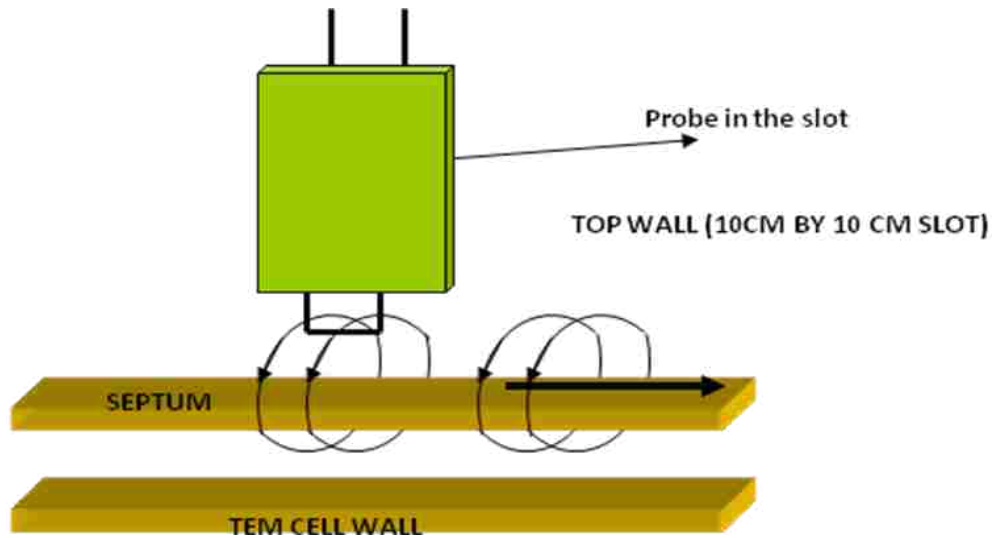Figure 2-14: TEM cell with the test board

Figure 2-15: Cross sectional view of probe placed in the TEM cell

2.4.6. Spatial Resolution Of A Probe. Spatial resolution of a probe can be defined as its ability to resolve the spatial variations of the fields near its tip or based on the smallest field change it can detect when moved sideways across the trace.

In case of a narrow trace the fields decay more as the probe moves higher above the trace. For a wide trace, on the other hand the fields are relatively homogenous; thus the probe cannot detect variations. To measure the spatial resolution of a probe, a narrow trace is required. When a probe is held at a particular height above a PCB-trace and moved across it the size of the loop determines the probe's spatial resolution. If two probes with different loop heights are held at same distance above the DUT, the probe with the higher loop couples extra field lines from much higher above the DUT (i.e., the

PCB trace). The response of the probe with a higher loop is flatter than that of a probe with a lower loop.

For measuring spatial resolution, a thin trace is required. The start frequency is set equal to the stop frequency. The probe is then moved across the trace equally in both directions.
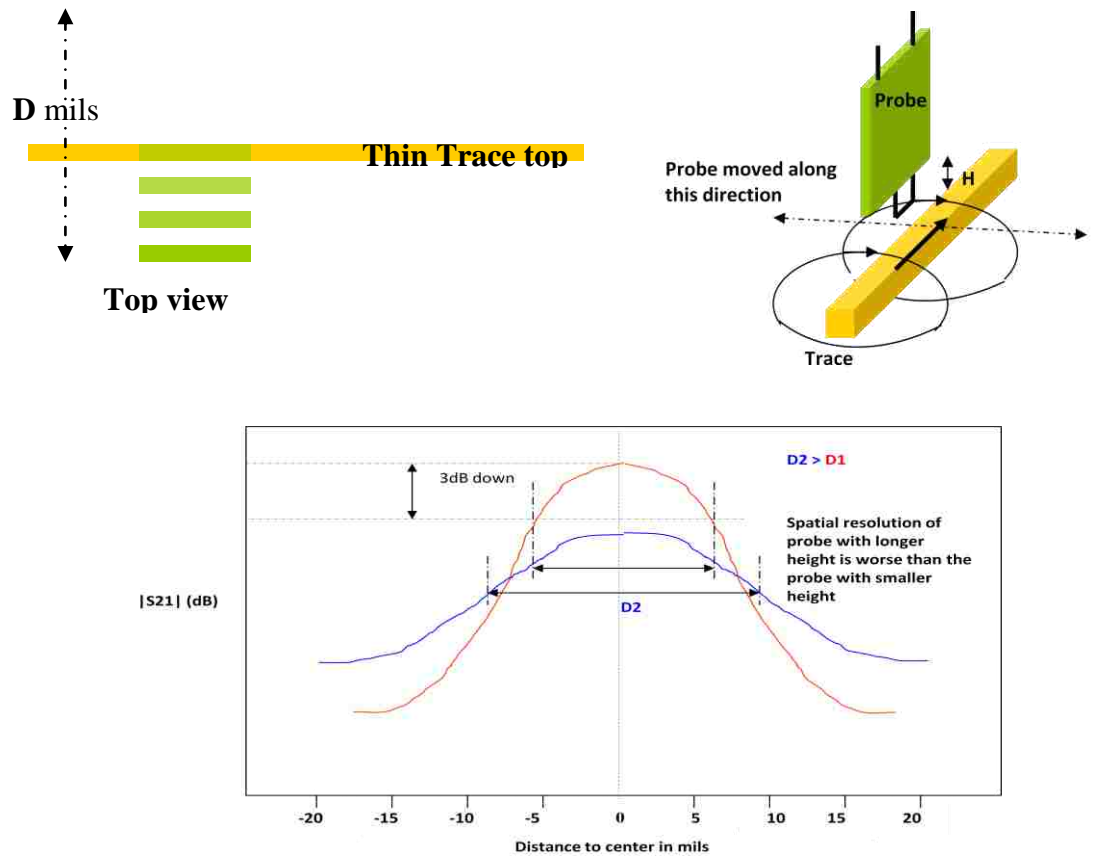

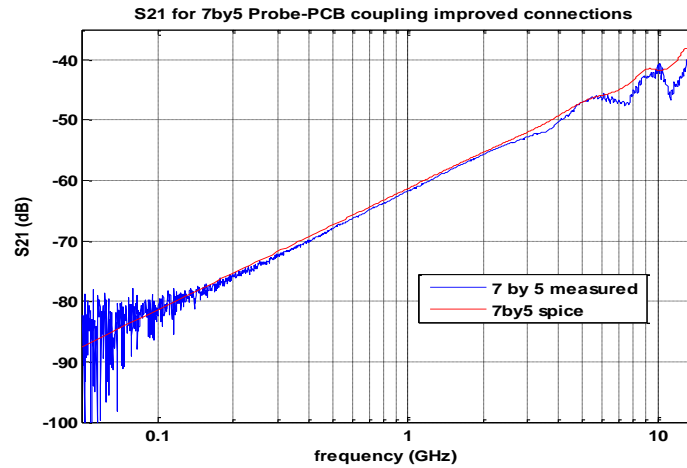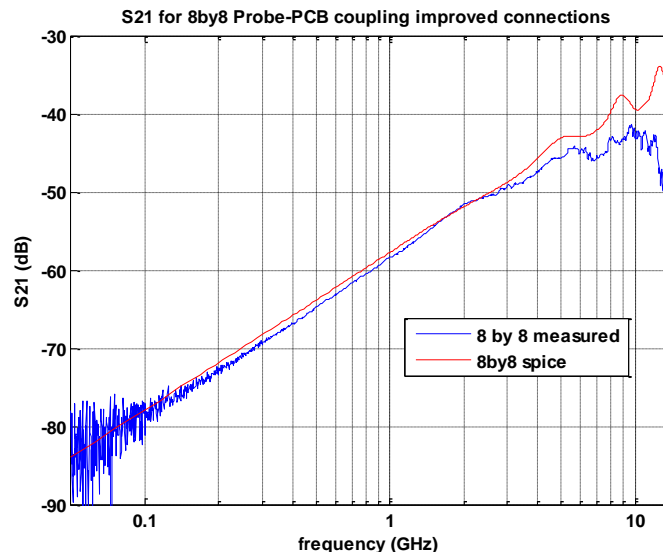Figure 2-16: Expected graph when probe is moved across a trace located at '0'

2.4.7. Frequency Response. Flex-circuit probes can be used to measure near-field EM radiations on fairly small PCB boards or circuits. The frequency response of the H-field flex probe typically rises at 20dB/dec, as shown in Figure 2-17(a).

(a)

(b)

Figure 2-17: S21for flex probes over trace: (a) 7×5 mil probe, (b) 8×8 mil probe

This property is a first-order derivative function in the time domain. If used in conjunction with an Agilent 1169 active probe the frequency response is flat above 30 MHz due to the low pass characteristic of the active probe's amplifier section.

Deviations at higher frequencies are explained by discontinuities or losses in the flex probe that were not taken into account in the calibration.

The resolution of the probe was not fully tested because the test structure could not be made small enough. A flex circuit trace would likely be needed to build such a structure. An IC lead frame might also suffice.

2.5. FLAT FREQUENCY RESPONSE

2.5.1. Motivation. A flat frequency response is desirable primarily for two reasons: First, such a response makes use of the A/D converter because many time domain impulsive processes have strong high frequency components (e.g., a fast rise and a slow decay). A probe that follows the derivative shows a narrow pulse of high amplitude at its output. The A/D converter settings (V/div) must be set to permit capture of the peak value. However, the deconvolution is an integration process for B-dot and D-dot sensors; thus, at lower frequencies signals that are small with respect to the full scale A/D converter are amplified by the deconvolution, reducing the accuracy of the results. In addition, a flat response reduces complexity in the calculations used to obtain the signal on a high speed digital circuit or PCB. In case of a flat frequency response, the system function decreases to a constant instead of a 20 dB per decade rise function. The following equation yields the signal in the frequency domain on the PCB circuit or the device to be tested:

$$S(\omega) = O(\omega) \big/ F(\omega) \tag{5}$$

where $O(\omega)$ is the frequency domain output from the system, $S(\omega)$ is the frequency domain signal on the DUT, and $F(\omega)$ is the frequency response of the probe that corresponds to the system function.

2.5.2. Agilent 1169A Active Probe. Typically, an active oscilloscope probe has a flat frequency response when used with its browser. However, this work found that the amplifier part of the active probe alone has a frequency domain response as shown in Figure 2-18. A low-frequency gain of 43.5 dB was observed until 31.8 MHz followed by a roll off of 20 dB per decade. The frequency response of the active probe is like an integrator that compensates for the first-order derivative response of flex probe, thereby giving a flat frequency response when combined with it.
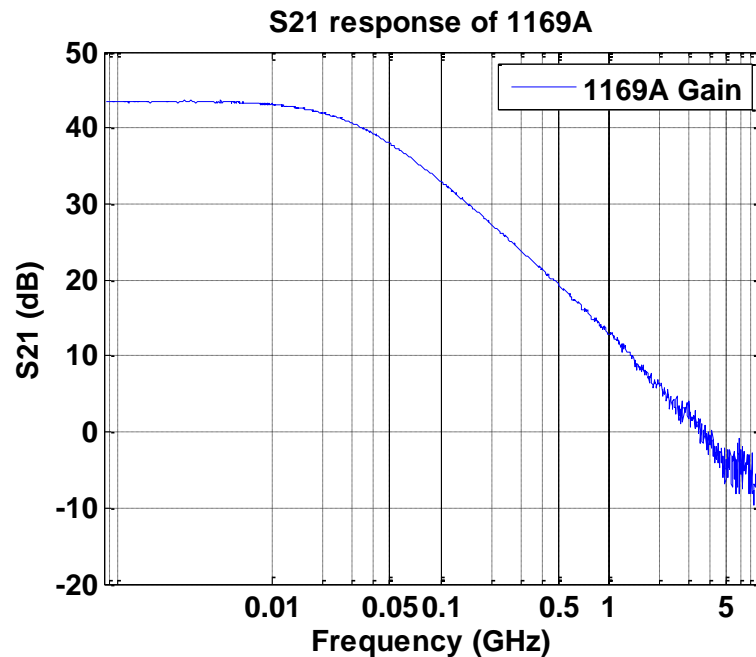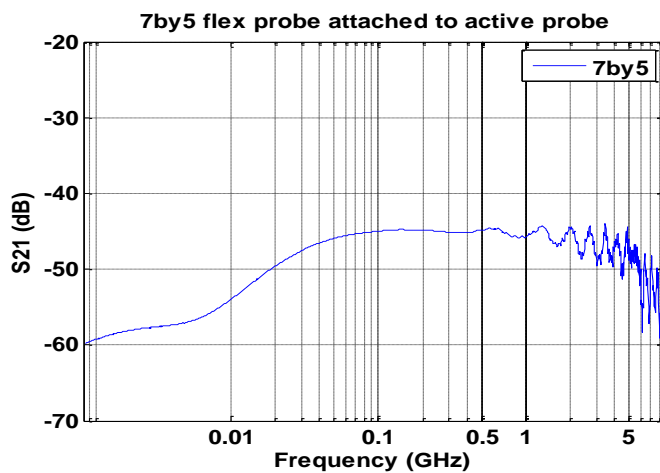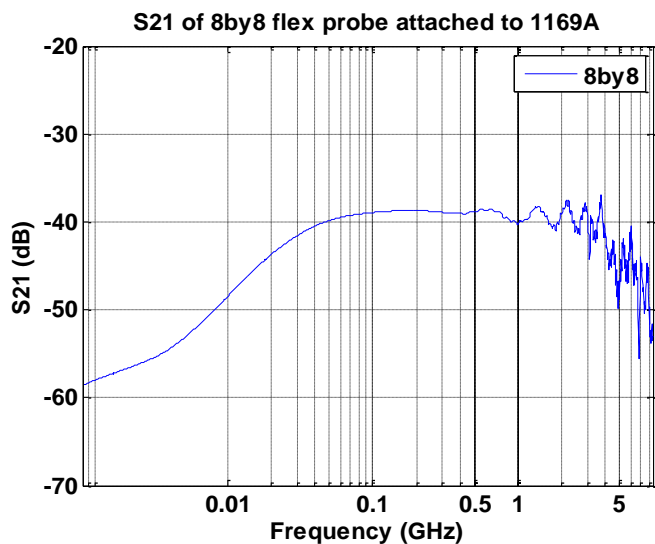

Figure 2-18: Gain of the Agilent 1169A active probe

2.5.3. Flat Frequency Response Results And Discussion. The measurement setup and method are discussed in the Appendix B.

(a)

(b)

Figure 2-19: Frequency response of the flex probes with 1169A coupled to trace: (a) 7×5 mil probe,(b) 8×8 mil probe

The results of measurement of the flex circuit H-field probes attached to the differential amplifier of the 1169A Agilent active probe are plotted in Figure 2-19 and discussed below.

Figure 2-19 shows the result as determined by the network analyzer. For the 7×5 mil flex probe, the frequency of the flex circuit H-field probe in conjunction with the active probe was quite flat after 60 MHz. As shown in Figure 2-19(a), the S21 of the 7×5 mil flex probe alone over the trace had a value of -83 dB at 0.1 GHz and -63 dB at 1 GHz. The active probe's S21, shown in Figure 2-18 was around 33 dB at 0.1 GHz and 14 dB 1 GHz. Their combination should result in a linear response of -50 dB from 31.8 MHz onwards because the active probe response starts to fall after that frequency. However, the flat frequency response actually began at 60 MHz, which could have been a consequence of the amplifier. The measurement results were found to be higher than expected as shown in Figure 2-19 (a). The reason for this could be that the probe itself was evaluated single ended, but if attached to the active probe's amplifier the difference is amplified, each channel by 43 dB at lower frequencies, leading to a 6 dB increased signal. The S21 was found to be higher than expected as shown in Figure 2-19 (a), perhaps because the distance of the probe to trace was not same in the two measurements. In this measurement the flex probe was held very close to the PCB trace but not in contact with it. The absolute value of S21 is a function of distance between the flex probe and the PCB trace beneath it. A mathematical deconvolution function can be written and implemented in the scope to flatten the frequency response maybe down to about 10 MHz.

2.6. E-FIELD PROBE

Appendix B describes the design of the bow tie antenna E-field probe. The probe was based on a bow tie antenna to make use of its wide bandwidth characteristics. The high-impedance loading of the active probe causes integration and hence a flat frequency response. The E-field probe was made from an electrically small dipole. It had to meet some requirements: First, the dipole had to be much shorter than the wavelength. Secondly, to achieve a flat frequency response, it had to be loaded by high impedance. The active probe meets these requirements.
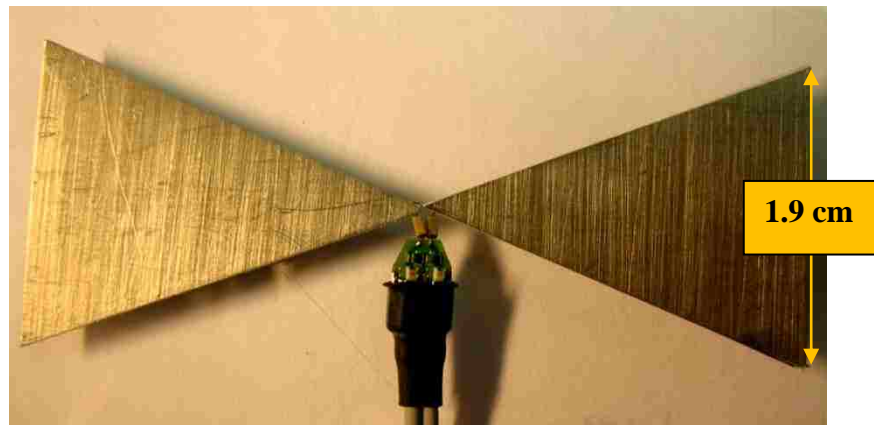

Figure 2-20: E-field probe based on bow tie antenna design

Figure 2-20 shows an E-field probe. An important difference between this and the H-field probe is that the active probe is used with its browser, not only its amplifier, to ensure a flat frequency response. An E-field probe loaded by high impedance already

has a flat frequency response, whereas an H-field probe needs an integrator to have such a response. The trade-off is sensitivity: The browser has a large attenuation. In principle, one could load the dipole directly with the active probe amplifier, thus increasing the sensitivity; however, the frequency response would be a 20dB per decade function.

For the present design, two triangle-shaped pieces of copper tape were soldered to the two tips (differential ends) of the browser of the active probe, forming a bow tie antenna. A bow tie antenna was used to make use of its high bandwidth characteristics. The size of the triangular copper was 1.9 cm wide at the end of the flare as shown in Figure 2-20. The E-field probe was then located at three positions inside the TEM line, as shown in Figure 2-21.
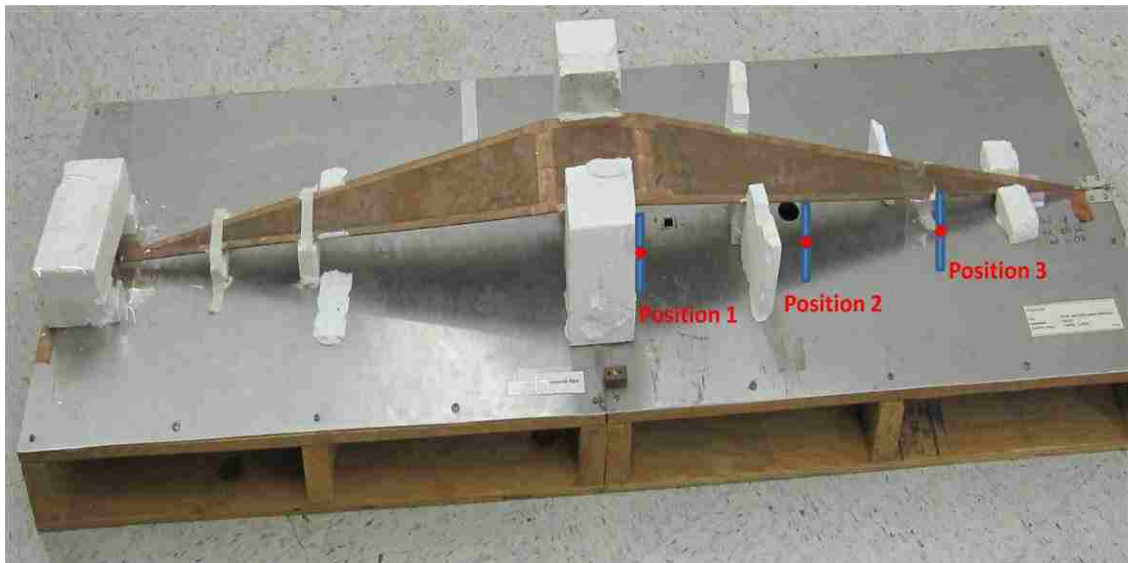

Figure 2-21: Open strip line cell for testing the E-field probe

Figure 2-22 shows resulting S21. The distance between the TEM line and the ground plane at position 1 was 10cm; the distance at position 2 was 8.5cm; and at position 3 it was 6cm. For each position, the S21 measured over a frequency range from 10MHz to about 2 GHz was quite flat as expected. When the distance between the strip-line and the ground plane was greater, the E-field between the two conductor pieces was smaller. At position 3, where the TEM line was 6 cm high, the S21 was much larger than expected because the probe's dimensions were comparable to the cell height (6 cm), which caused field disturbance.

The lower cut-off frequency was about 10 MHz. It was set by the impedance of the active probe and the capacitance of the probe and the browser.

The ripples beyond 1 GHz were most likely not a result of the E-field probe, but a consequence of reflections within the TEM cell.

The sensitivity of the E-field probe can be expressed as:

$$Sensitivity = \frac{V_{outputof\ probe}}{E_{field\ in\ Volts/meter}}$$

(6)

where $V_{output\ of\ probe}$ is the output voltage of the probe; $E_{field\ in\ Volts/meter}$ is the electric field inside the TEM cell.

Sensitivity of the E-field probe was found to be 3.3 mV/(V/m). The steps followed to calculate the sensitivity is described in Appendix C.
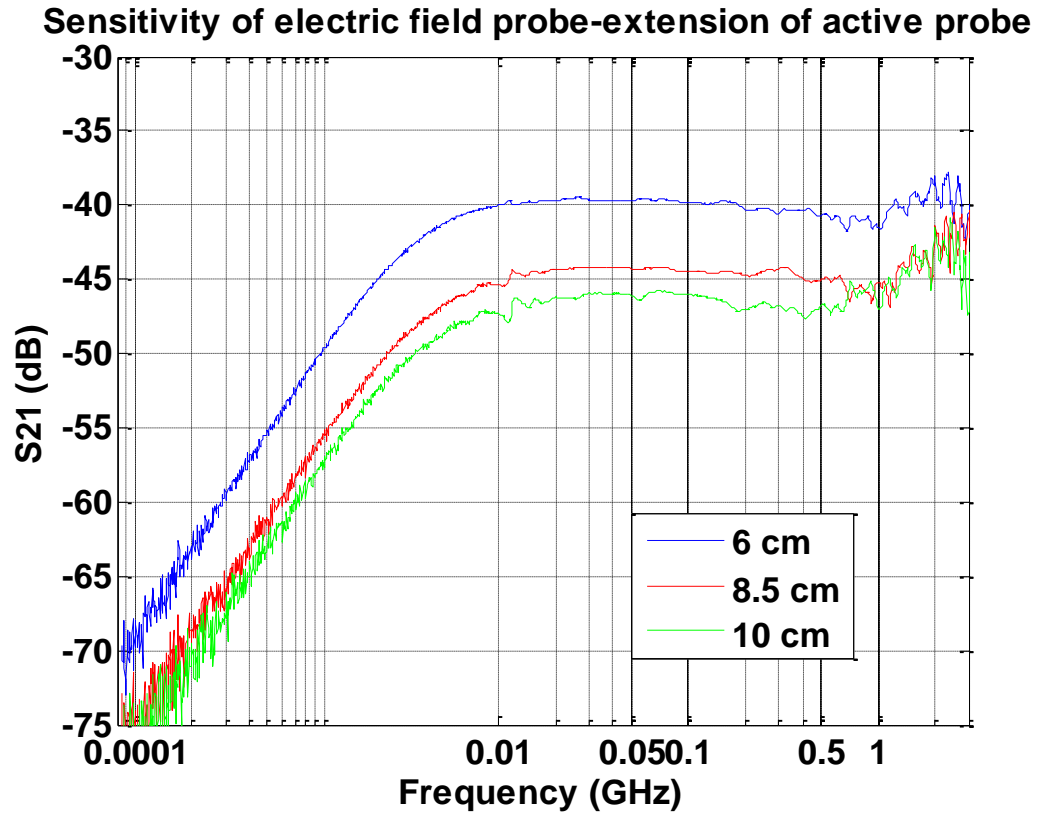
Sensitivity of electric field probe-extension of active probe

Figure 2-22: S21 of the E-field probe

3. 1-MIL PROBE DESIGN

3.1. INTRODUCTION

In this project the H-field 1-mil probe was designed to increase sensitivity without sacrificing spatial resolution. Chapter 2 explained that the flex circuit H-field probes have high spatial resolution but low sensitivity due to their smaller loop size. The smallest probe available is 3×3 mil and the largest loop size is 8×8 mil. To improve the sensitivity three-turn flex-circuit H-field probes were designed but were not built due to time and financial constraints. By increasing the number of turns in the loop, self-inductance increases, which in turn increases coupling coefficient.

This project developed a novel method to improve the sensitivity of the probe by changing its material properties rather than by increasing the number of turns in the probe. Magnetic field coupling can be significantly improved by increasing the relative permeability of the material. Magnetic field lines are more concentrated in a higher permeability (μ) material. The H-field 1-mil probe is a four-layer PCB structure in which the traces run in the second and the third layers and are connected by a buried via near the tip of the probe. The relative permeability of the probe is changed from 1 to 300 to observe the difference in sensitivity. The sensitivity increases but the self-resonance of the probe decreases because of increase in self inductance as explained in detail in the Chapter 2.

This section discusses the results of the full-wave simulation of the probe coupled to the PCB trace beneath it.

3.2. VALIDATION OF FULL-WAVE MODELING OF THE 1-MIL PROBE

  A new method was established to validate the simulation results of the 1-mil H-field probe. A comparison between simulation and measurement results of trace coupling frequency response of the 7×5 mil flex circuit H-field probe was done for validation of results followed by estimating the sensitivity of the 1-mil probe at a given frequency. This estimate was then compared with the results of the simulated 1-mil probe. Equation 4 above provides a good first order estimate of the sensitivity of loop probe. The method for validating the full-wave modeling of the 1-mil probe involves the following steps:

- The trace coupling frequency response of the 7×5 mil flex circuit H-field probe was measured using the Network Analyzer.

- The distance of the probe tip above the microstrip trace (DUT) was measured.

- A full-wave simulation of the 7×5 mil flex-circuit H-field probe coupled to the same microstrip trace was performed.

- To model the microstrip trace, its geometry and material properties were extracted using the ADS line calc feature of the advanced design system (ADS) tool provided by Agilent.

- The frequency response of the 1-mil probe coupled to the same microstrip trace (DUT) was simulated in full-wave.

- The 1-mil probe response was predicted based on the frequency response of the flex-circuit probe.

- If this prediction matched the simulation results; then the modeling could be considered valid.

3.3. FULL-WAVE SIMULATION RESULTS

Figure 3-1 shows the full wave model of the 7×5 mil flex-circuit H-field probe manufactured as part of this project and discussed in Chapter 2. The frequency response of this full-wave model was validated by comparing it with the measured results for a probe coupled to a microstrip trace. The PCB trace used as a DUT was a 50 Ω microstrip. The dimensions of the microstrip were measured using a digital caliper, and its dielectric constant was synthesized by specifying the other parameters using the line calculation operation provided by the ADS circuit simulation tool. The trace coupling response of the probe was measured using a network analyzer. The measurement procedure is described in detail in Appendix C.
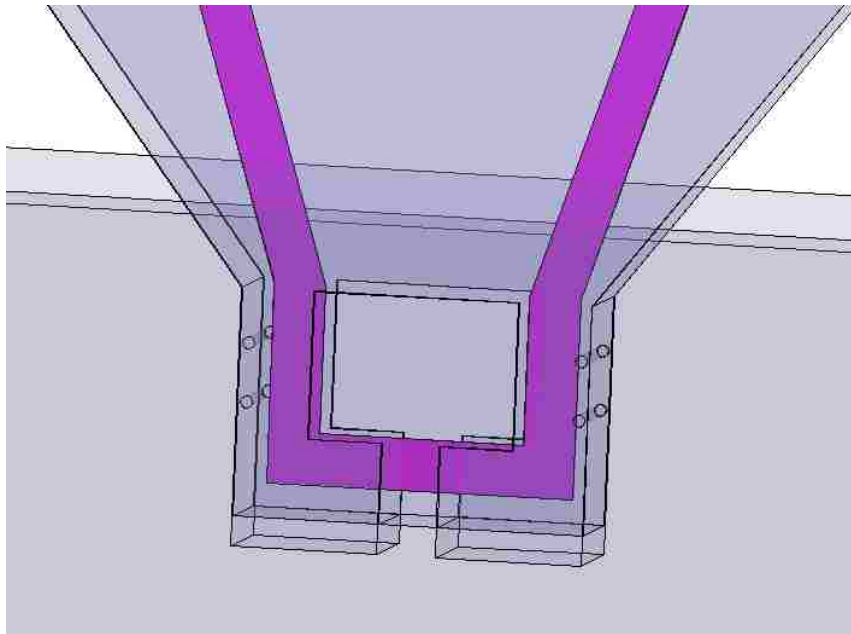

Figure 3-1: 7×5 mil flex-circuit H-field probe full-wave model

Noncontact probes such as the flex-circuit H-field probe are very sensitive to the distance from their tip to the PCB trace (DUT) below. Here, the distance was estimated and used in the full-wave modeling. Figure 3-2 compares the measured and simulated results for the 7×5 mil flex-circuit H-field probe coupled to the 50 Ω microstrip trace. The simulation results agree closely with the measured results, validating the full-wave model. The red and green curves represent the simulation results and the S-parameters between ports 1 and 2 of the differential flex-circuit probe and the microstrip trace beneath.
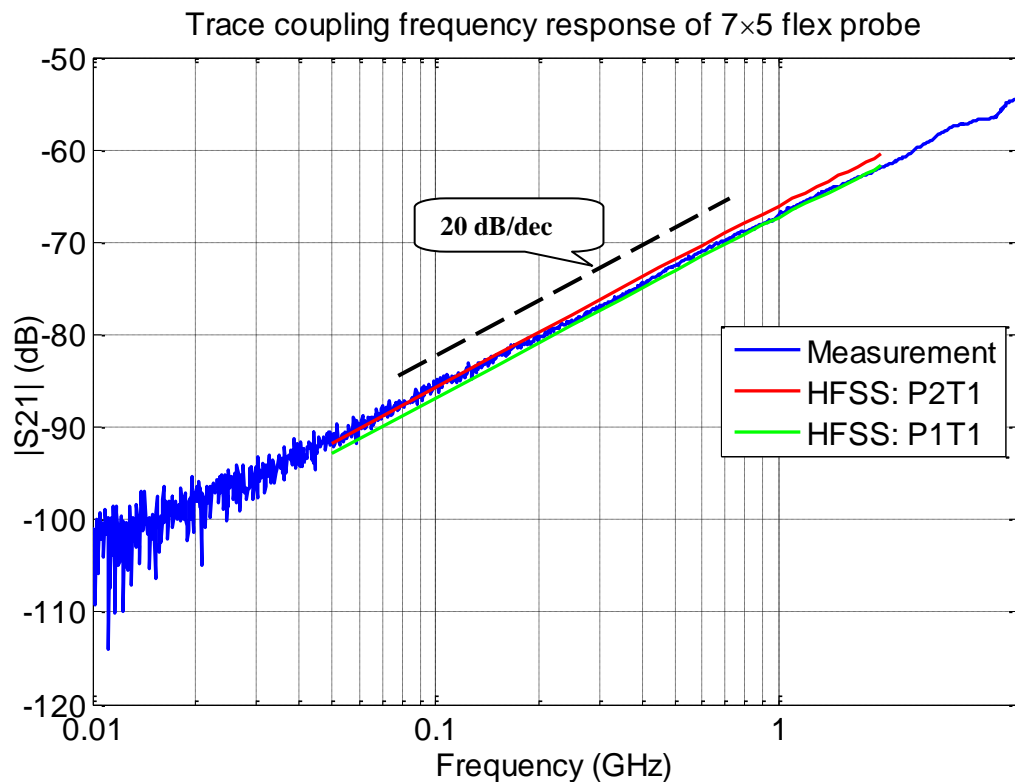

Figure 3-2: Trace coupling frequency response of the 7×5 mil probe

Figure 3-3 shows the full wave model of the 1-mil probe. A cut was made across one of the GND planes to break the continuity in the loop formed by the outer shield. This was done to avoid eddy losses. The value of S21 for the 1-mil probe was predicted to be -116.38 dB at 100 MHz. The simulation results show a value of -114 dB, as indicated by the light blue curve in Figure 3-4. The simulation result agrees closely with our expectation, thus validating this simulation. When the overall size of the 1-mil probe was reduced, the resonances are shifted higher in frequency. The two green curves are the trace coupling response at the two differential ports of the probe. Both tend to start bending at about 1.5 GHz. The blue and red curves are for the shorter length probe and the curves do not bend until 2 GHz and higher. The deviations occurring at high frequency in the curve were the result of dielectric losses, which are more dominant at higher frequencies. The dielectric losses decreased when the size of the probe was reduced, as shown in Figure 3-6. Hence, the deviations in the trace coupling response were shifted to a higher frequency.

Figure 3-5 shows the full-wave models of the 1-mil probe at two different sizes. The insertion loss of the full size probe in Figure 3-5 (b) is depicted by the blue curve in Figure 3-6. Clearly the bigger probe has higher insertion loss and hence more deviations in the frequency response shown by the two green curves in Figure 3-4.
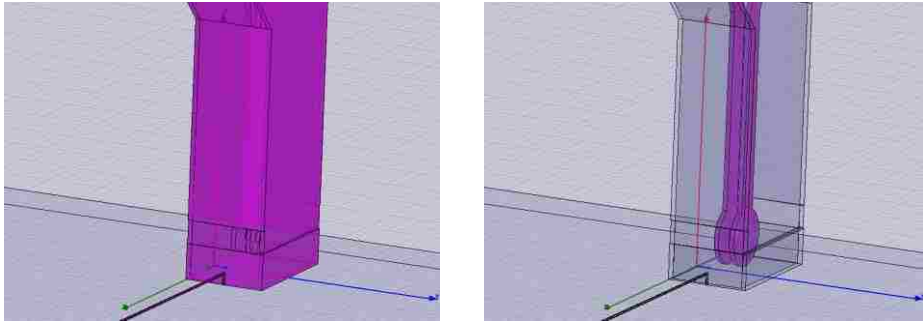
Figure 3-3: Full wave model of 1-mil probe showing the cut across one of the GND planes to avoid eddy losses.
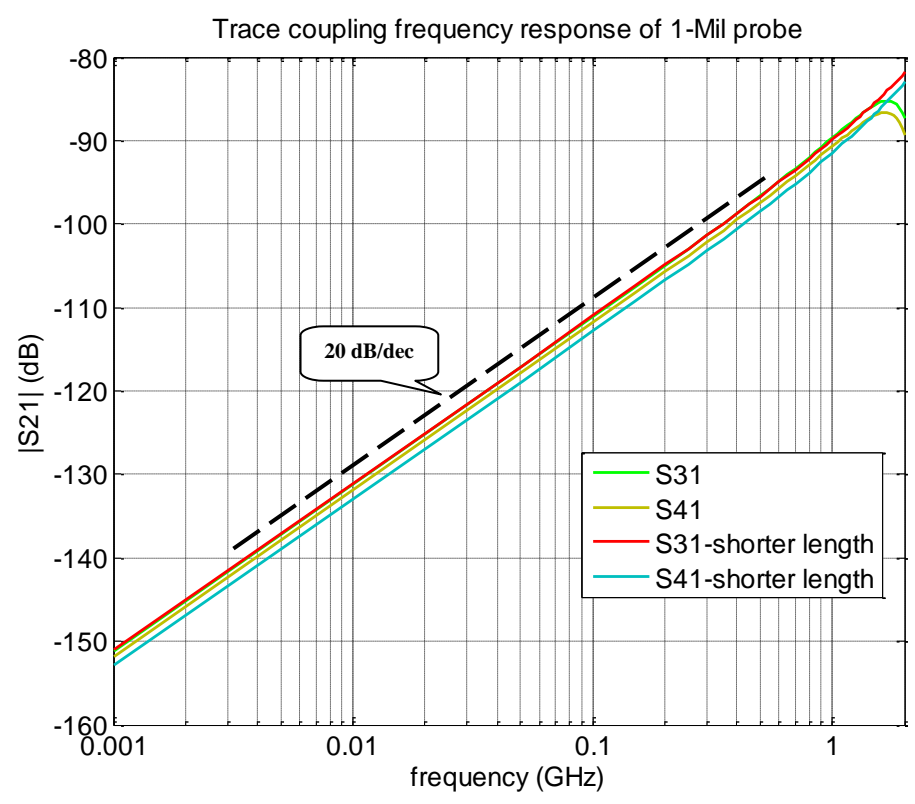

Figure 3-4: Trace coupling frequency response of the 1-mil probe over the same DUT used for the 7×5 mil flex circuit H-field probe
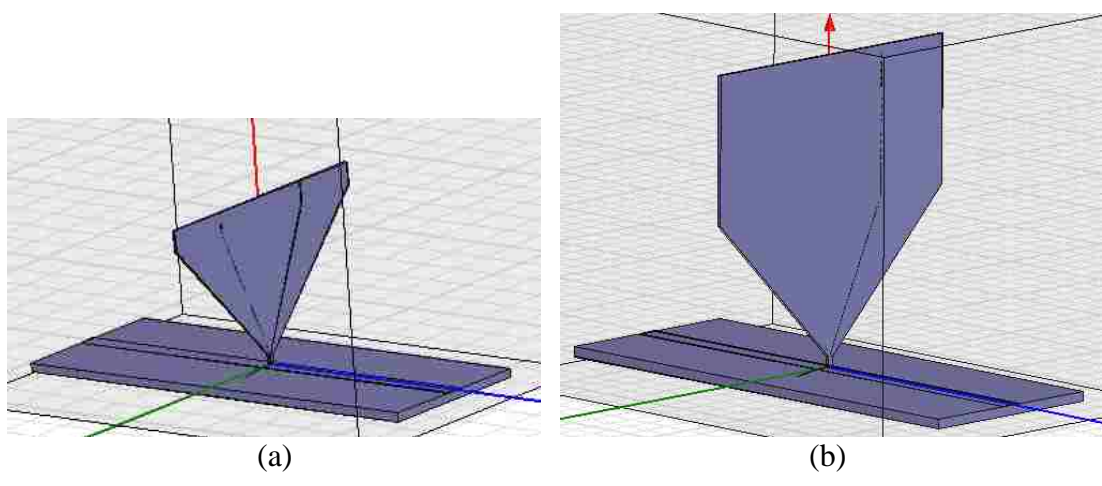
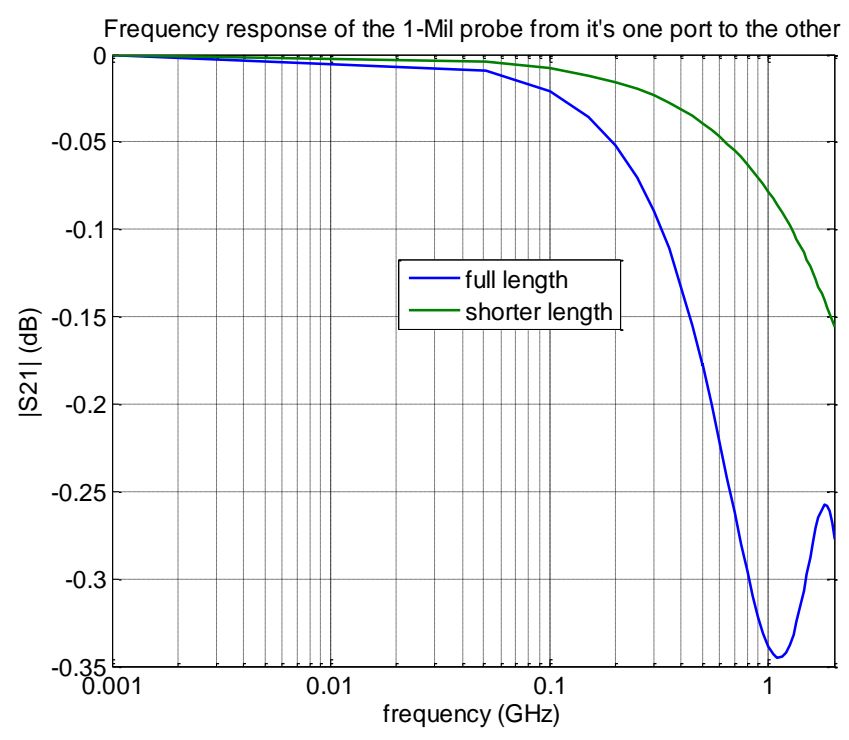Figure 3-5: Full wave models of 1-mil probe: (a) small probe, (b) full-size probe

Figure 3-6: Frequency response of the 1-mil probe from one port to the other for
two different sizes

Figure 3-7 and Figure 3-8 illustrate the spatial resolution of the 7×5 mil flex-circuit H-field probe and the 1-mil probe. The probes were held at 2 mils height above the PCB trace and moved across in x-direction. Horizontal components of the H-field were captured in this process. Spatial resolution of the 1-mil probe was 110 μm and that of the 7×5 mil probe was 275 μm. Physical significance of spatial resolution is the ability of the probe to distinctly resolve the field lines in space. More number of H-fields lines pass through a larger loop thus making it difficult to resolve each distinctly.
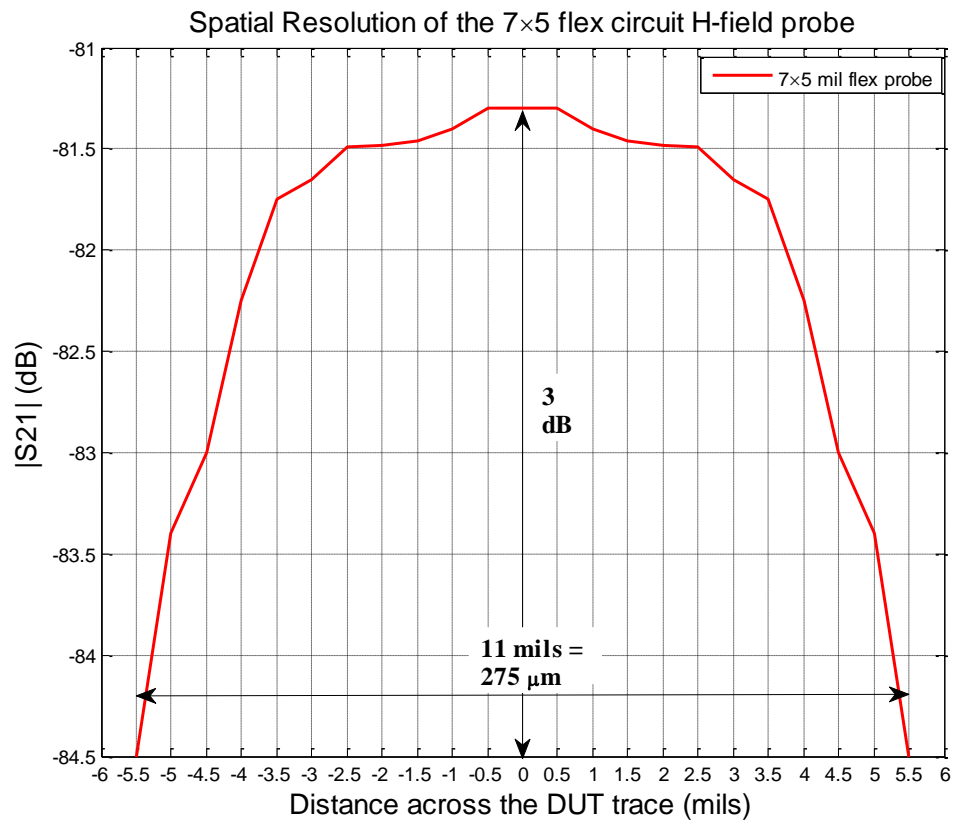

Figure 3-7: Spatial resolution of the 7×5 mil flex-circuit H-field probe over a thin DUT trace

The field lines at 2 mils height above the microstrip trace tended to become vertical at 3 mils distance across the PCB trace (i.e., in x-direction), thereby nullifying the horizontal component of the H-field. Thus two null points at 3 mils distances on each side of the trace were observed as in Figure 3-8.

After the two null points, the field lines had a tendency to change direction thus inverting the horizontal component of H-field and causing phase inversion as seen in the graph for 1-mil probe. The 7×5 mil probe did not detect the null points because it was unable to resolve the field lines distinctly. Even at 3 mils distance across the trace, there were some other field lines entering its loop due to its larger size and hence it measured some field. So, no null points were observed in its graph in Figure 3-7.

To validate the simulation results of spatial resolution of the 1-mil probe, fields were calculated for an ideal-point like source over an infinite ground plane for the same relative distances used in full wave simulation. Image theory was applied to take care of the ground plane. Superposition rule was applied to find the effective horizontal components of magnetic field (Hx) at a height of 2 mils above the trace

The plot for calculated H-field is shown in Figure 3-9. The Hx tends to become extremely low at 3 mils distances across which is similar to the trend observed in Figure 3-8. But the change in the magnetic field is roughly 10 dB in the fields found from image theory analysis which is much larger than the simulation results.

Thus, at a height of 2 mils above the PCB trace, the variation in magnetic field on top of the trace and at 3 mils distance across the trace was expected to be much higher than the simulation results as shown in Figure 3-8. This needs to investigated in future.

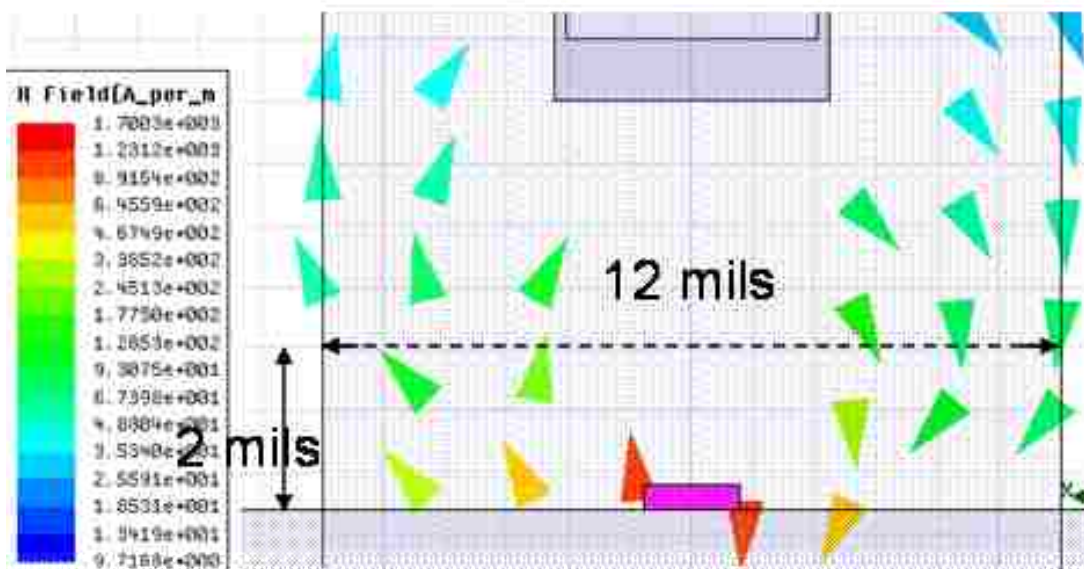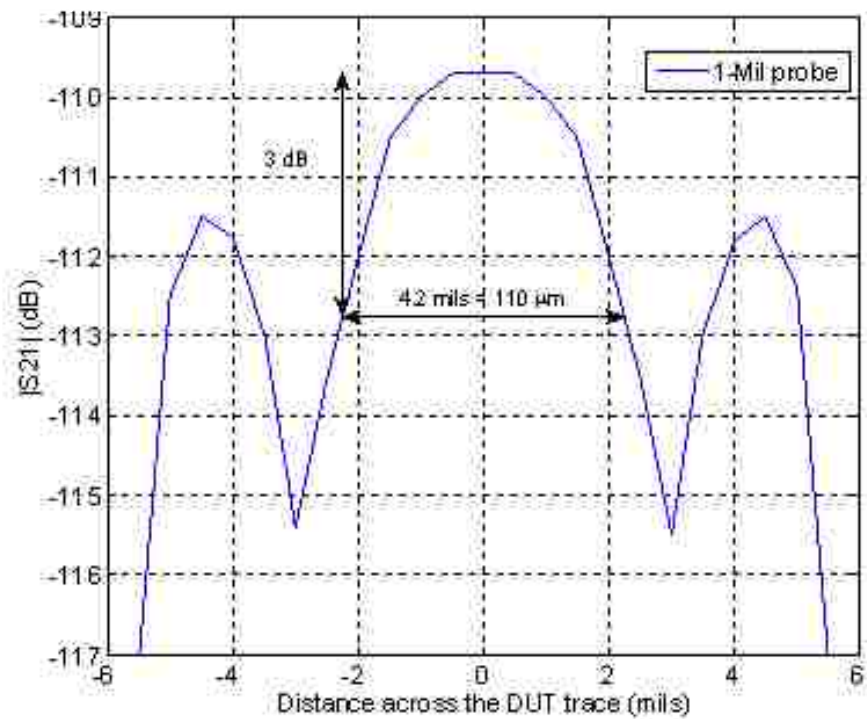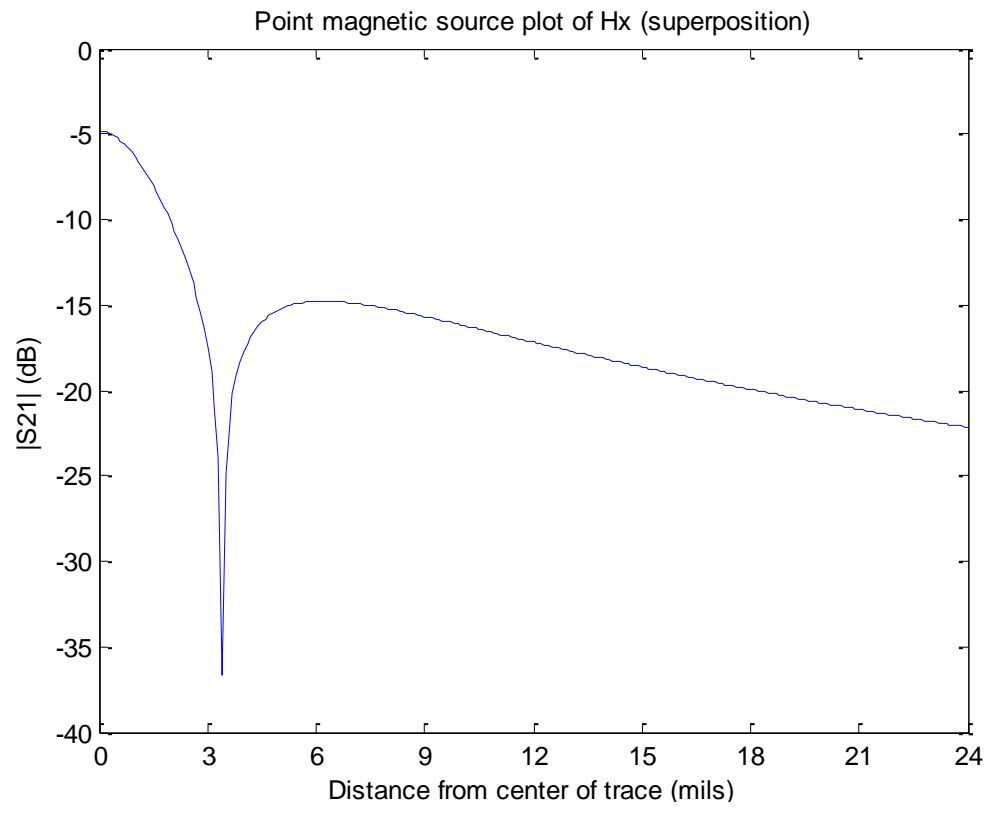Figure 3-8: Spatial resolution of the 1-mil probe over a thin DUT trace

.

Figure 3-9: Horizontal component of magnetic field for an ideal point like source for same relative distance as the simulation for the 1-mil probe

4. CONCLUSIONS AND FUTURE WORK

A new approach to calculate the TWDP value of a channel based on its frequency-domain S-parameter data was presented. The new approach provided many advantages over the conventional approach, such as reduced cost, improved repeatability, reduced setup complexity, and better accuracy. A parametric study on TWDP with respect to some setup parameters was also reported. The results indicated that the TWDP value increased with the increase of frequency and the decrease of the rise/fall time. The results also depicted that higher samples per bit and pattern repetitions would be needed to obtain accurate and repeatable TWDP value.

The flex-circuit H-field probes were developed and characterized. They were characterized as stand-alone and in combination with the differential amplifier of the 1169A active oscilloscope probe. Active oscilloscope probes can be found in many labs. They can be extended to be used as field probes achieving a flat frequency response for the E-field, independent of the manufacturer of the active probe and a flat frequency response of for the H-field probe above approximately 50 MHz if a specific probe is used. The article showed the implementation and measured results of small H-field probes, manufactured in flex circuit technology having loop dimensions as small as 3x3 mil. Flex-circuit technology allowed manufacture of fine probes hence higher spatial resolution was achieved. The probe worked well upto about 3 GHz.

The 1-mil probe design was validated and is ready to be manufactured. The probe has four layers and its loop lies in the cross-sectional plane of the PCB board. Hence it was possible to achieve such a small loop size. It was designed to increase the sensitivity of the probe without compromising the spatial resolution by using a high permeability

material as the dielectric. Using such a material allows crowding of magnetic field lines in the dielectric thereby increasing the voltage induced in the loop of probe. However, the high permeability material is currently not available for manufacturing, so, the full wave model for the 1-mil probe was developed for a relative permeability of dielectric of 1. The simulation results for this probe were validated based on expectation drawn from the simulation result of the 7×5 mil flex-circuit H-field probe. The expectation was in close agreement with the simulation. Hence the 1-mil probe design was validated. It was designed and is in the process for manufacturing.

APPENDIX A
TWDP CALCULATOR TOOL DESCRIPTION

TWDP/LPA Tool

This appendix illustrates the various features of the TWDP/LPA simulation tool and demonstrates its operation

✓2-port
✓ 4-port single ended
✓4-port differential ended

✓User Friendly

Flexible S-Parameter Inputs.

User Defined Bit Rate

✓User Friendly

Cascaded S-parameters

Number of Samples per bit

✓More than one S-parameters can be cascaded together

User defined Input Signal

Variable Rise/Fall times

✓CJTPAT
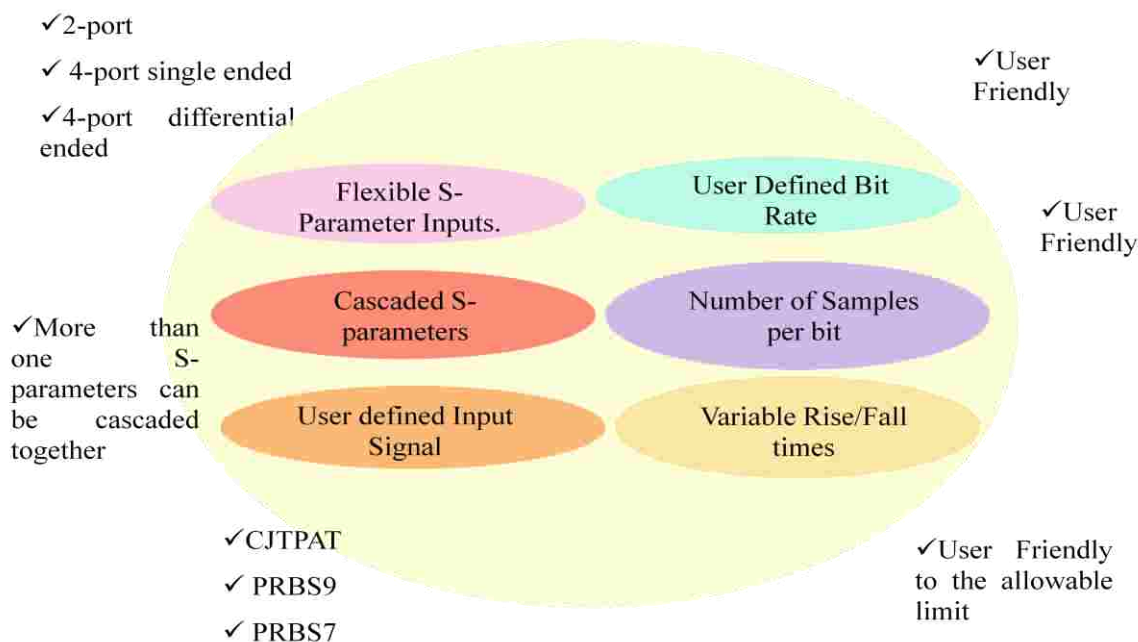✓ PRBS9
✓ PRBS7

✓User Friendly to the allowable limit

Figure A.1: LPA tool features

Figure A.1 shows a diagram illustrating the various features of the TWDP/LPA simulation tool. The tool accepts 2-port, 4-port single ended and 4-port differential ended S-parameter files.

It permits cascading of S-parameter files. Various input sequences can be generated including CJTPAT, PRBS9, and PRBS7. A user-defined sequence can be loaded.

Recently, changes have been made to this tool to permit implementation and emulation of jitters in the transmitter. Nitin Radhakrishnan, my colleague from EMC lab introduced Jitter analysis to the TWDP/LPA simulation tool while he was working on the project with my Advisor Dr. Jun Fan. (Nitin Radhakrishnan, 7/29/2009)

The tool allows variable bit rates, rise/fall times, and numbers of samples per bit. (For a study on the TWDP parameter these parameters were varied and results plotted and discussed over.)

Operation of TWDP simulation tool:

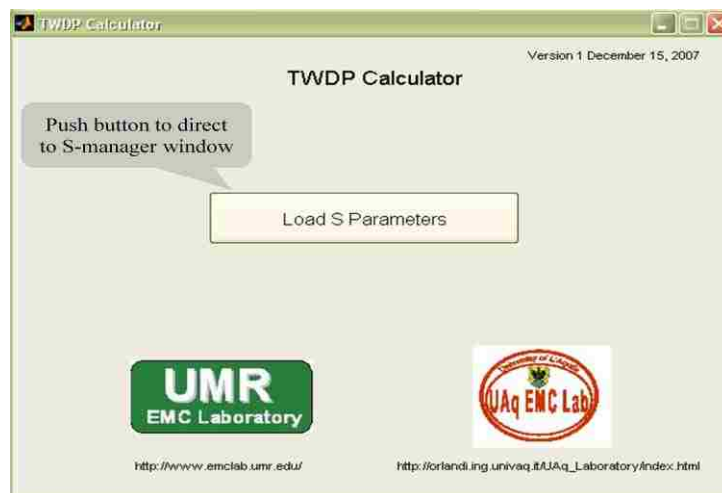Load S-parameters by clicking on the button in the startup GUI shown in Figure A.2.

Figure A.2: Load S-parameter window

Click on the button "Next Cascade" in the S-parameter window shown in Figure A.3. A drop down list appears from which to select the required scattering parameters can be selected. This work generally used the transfer parameter S21 to find TWDP. The waveform button is thus enabled.
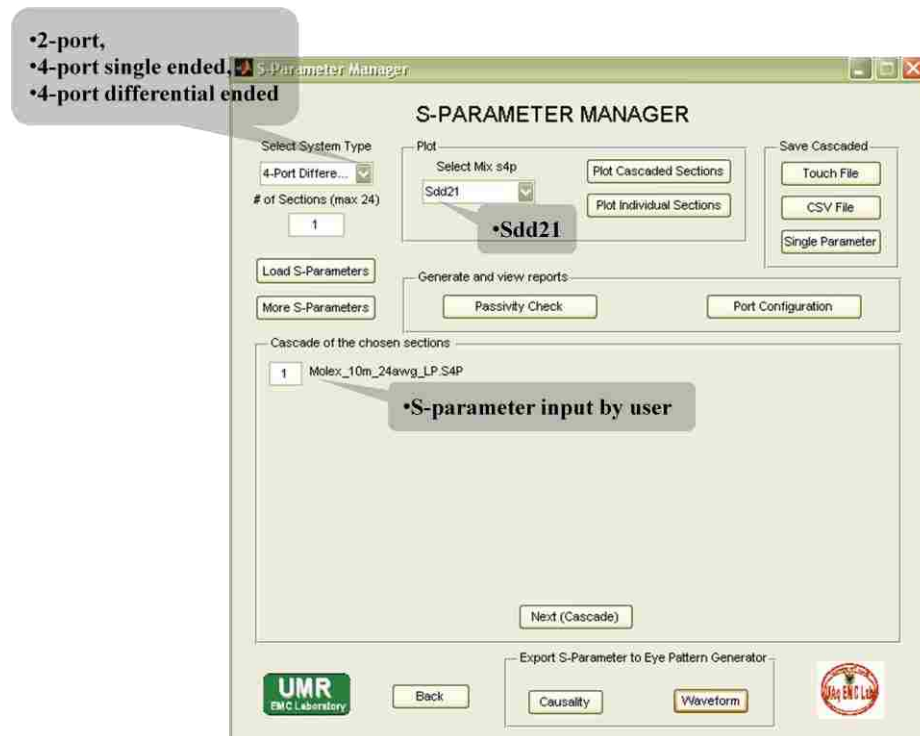

Figure A.3: S-parameter manager window

By clicking on the plot cascaded/individual sections, the S parameter characteristics of the channel or DUT can be plotted. Figure A.4 shows an example of this feature for Molex cable.
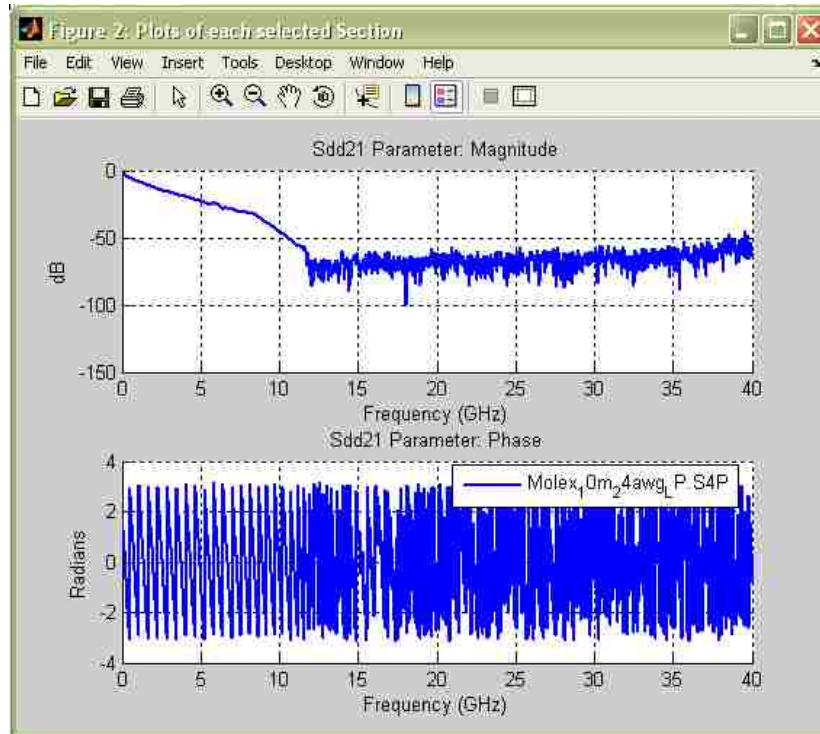
Figure A.4: Plot S-parameter window

Click the waveform button to be directed to the waveform generator window shown in figure A.5. Various parameter can be changed to suit the user's needs.
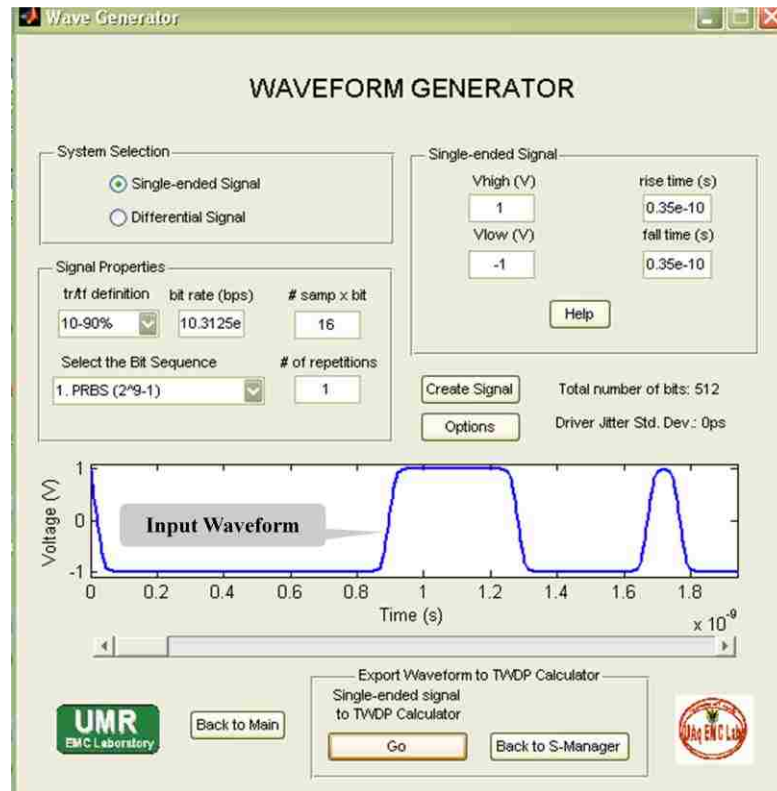
Figure A.5: Waveform Generator window

The waveform is then exported to the TWDP calculator where complex analytical computations are performed to obtain the final TWDP result.
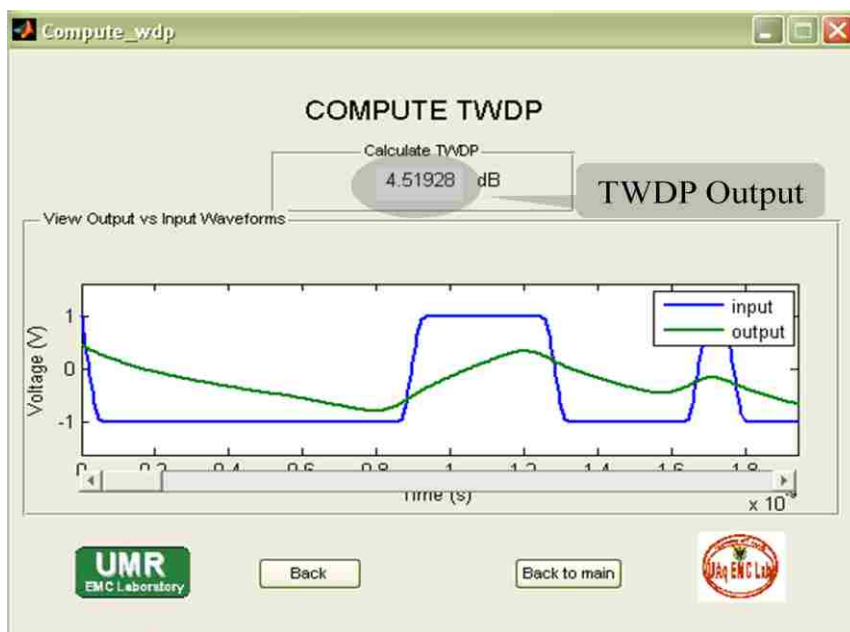
Figure A.6. TWDP value display window

APPENDIX B

FLEX-CIRCUIT H-FIELD PROBE AND E-FIELD PROBE DESIGNS

The following describes the design of flex-circuit H-field probes and shows the probes available in the EMC laboratory, at Missouri University of Science and Technology.

Probes manufactured and available: Flex Circuit probes are available in five sizes:

- 3×3 mil

- 5×5 mil

- 7×5 mil

- 8×8 mil

- 5×5-T_slot

The difference between 5x5 mil T-Slot and 5by5 probes is that the whole loop area of the latter is exposed to the magnetic fields whereas in the former a T-shaped slot is made as shown in Figures B.1 and B.2. An experiment has been designed to compare the sensitivities of the two probes; however, it has not been performed yet.

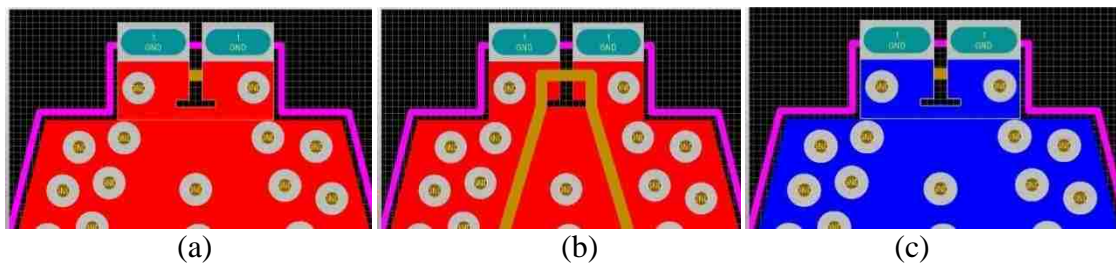<center>(a)   (b)   (c)</center>

Figure B.1: 5×5-T_slot flex probe: (a) Top layer, (b) middle layer, (c) bottom layer
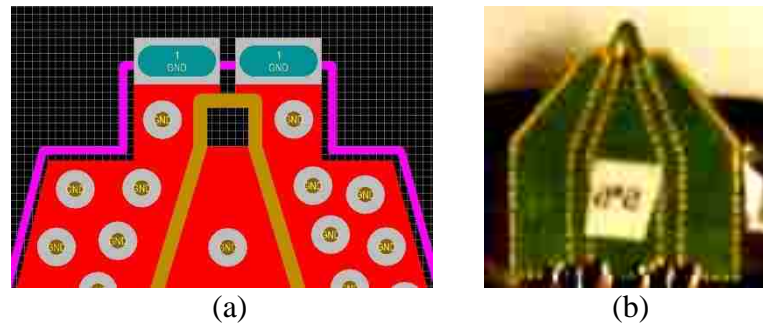
Figure B.2: Layout of manufactured 5×5 flex probe with complete 25 mil^2 area exposed to H-fields: (a) layout, (b) photograph of manufactured probe

The first four probes listed above have been characterized and tested. The 5by5-T_slot probe, however, has not yet been tested.

Five sizes of a 3 turn probes have also been designed thus far. They have not yet been manufactured, however, because manufacture and characterization of the single-turn probes had first priority.

Three turn flex probe design: The three-turn probes were designed in five sizes:

- *10×7 mil*
- *10×8 mil*
- *12×4 mil*
- *12×12 mil*
- *15×15 mil*

Figure B.3 shows the layout of the 10×7 mil probes, the smallest design. It shows different layers.

(a)   (b)   (c)

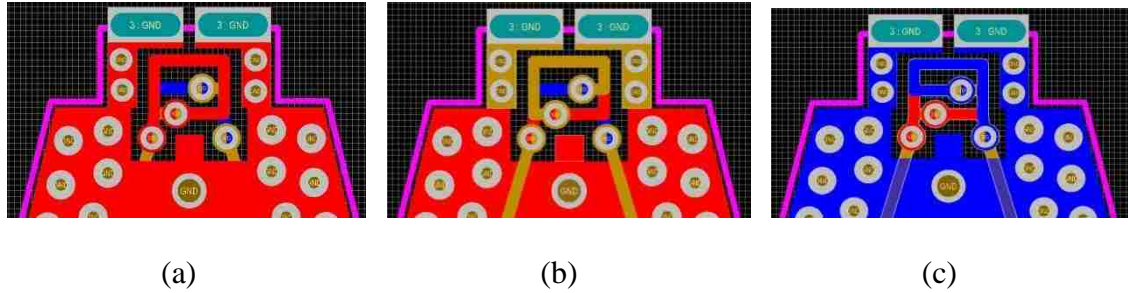Figure B.3: 10×7 mil three-turn flex probe; (a)Top layer, (b) Middle layer, and (c)
Bottom layer

1. In Figure B.3 the differential traces run along the middle layer.

2. At the top, the trace on the left is connected to the trace on the top layer (shown in red)

through a blind via, which then makes a turn in the top layer and is connected to the trace

3. running in the middle layer through another blind via.

4. The trace in the middle layer makes a second turn in the middle layer itself and then

connects to the trace in the bottom layer using the third blind via.

5. This trace is now connected to the differential trace on the right in the middle layer.

E-field probe design:

The E-field probe was designed based on a bow tie antenna.

Figure B.4: E-field probe based on bow tie antenna design attached to active probe browser

The Figure B.4 shows the E-field probe. The tips of the browser of the active probe are attached to a bow tie antenna. The two triangular PCB's are soldered to the browser tips. The whole probe structure is placed on plexi-glass. The integration is achieved by the high impedance loading of the active probe's browser.

APPENDIX C

FLEX-CIRCUIT PROBE CHARACTERIZATION: MEASUREMENT SETUPS

AND PROCEDURES

TIME DOMAIN REFLECTOMETRY [TDR] CALIBRATION AND RESPONSE

OF FLEX-CIRCUIT H-FIELD PROBE

This procedure describes the calibration steps required before TDR testing to reveal the circuit topology of the flex -H-field probe and the PCB trace (i.e., the DUT).

This procedure is applicable to the Missouri University of Science and Technology (Formerly University of Missouri Rolla) Electrical and Computer Engineering.

It relies on an Agilent 86100C Digital Communications Analyzer (DCA)

Calibration Steps:

- Set up the 86100C DCA by turning the power switch to ON. Allow the analyzer to run for approximately 30 minutes to stabilize it before attempting calibration.

- Press the "Default setup" button found on the right side of the front panel.

- Press the "TDR/TDT Mode" button (see the Figure B.1).

- Press the "TDR Setup…" on the left side of the main screen. A new window (TDR/TDT Setup) will open.

- Press the "calibration wizard" button. A small window with calibration instructions will appear.

Figure C.1: TDR Instrument Details

Calibration:

- Ensure that "TDR cal on channel 1" is selected.

- Depress the "next" button.

- Ensure that left module vertical calibration is selected.

- Depress the "next" button.

- Disconnect everything from left module (all terminations), and press "continue."

- Connect a 50 Ω load to channel 1, and press "continue." Wait for the TDR instructions.

- Disconnect everything from the left module. Then press "continue," and wait for the TDR instructions.

- Adjust time base for TDR cal on channel so that the entire response is visible press "set up"

- Enter time per one division and close the window. Delay remains at default value press "next"

TDR Cal on channel 1

- Connect short to channel 1, and press "next." Wait for next TDR instructions.

- Connect 50 Ω load to channel 1, and press next

- Follow TDR instructions. If calibration is completed, press "finish."

- Do not change effective rise time.

- Close the TDR/TDT setup window.

TDR RESPONSE OF FLEX CIRCUIT H-FIELD PROBES.

- Connect one end of the differential flex-circuit H-field probe to channel 1 of TDR, and terminate the other end in a 50 Ω load.

- Adjust the time base for best scope presentation.

- Zoom In the portion of the response that represents the existing parasitics of the probe and that are developed by connecting the probe to the coaxial cable.

- Measure the parasitics as shown in Figure C.2

  - ✓ Place the two markers of the TDR at the start and end of the transition.

  - ✓ The values then displayed in a small pop-up window are the corresponding parasitics.
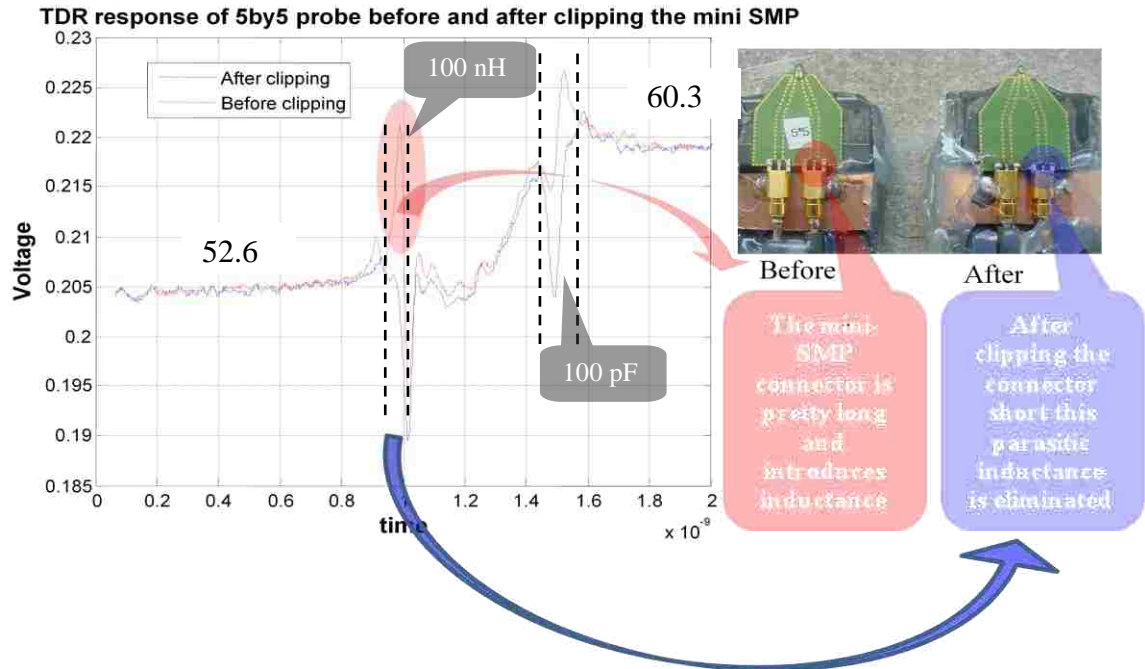
Figure C.2: TDR Response

FREQUENCY DOMAIN RESPONSE OF FLEX CIRCUIT H-FIELD PROBES

This procedure describes the calibration steps required before measuring the PNA network analyzer frequency response measurements of the flex-circuit H-field probes.

It is applicable to the Missouri University of Science and Technology Department of Electrical Engineering.

The process relies on an Agilent E8364B PNA Network Analyzer (10MHz to 50GHz) and an Agilent N4693-600003 Electronic Calibration Module.

Calibration steps:

- Ensure that both the "Line switch" and "Power switch" of the Agilent E8364B
  PNA Network Analyzer are ON.

- Press the 'Preset' button found in the UTILITY section of the PNA front panel.

- Enter the frequency range of interest for calibration.

  - Click on the menu option 'Channel' from the main menu bar of the PNA
    screen

  - Choose the option 'start/stop' from the drop down menu.

  - Enter 10 MHz as the start frequency and 10 GHz as the stop frequency; click
    'OK'

- Enter the number of sampling points.

  - From the main menu bar of the PNA screen, click on the menu Option
    'sweep.'

  - In the drop-down menu, click on the option "No. of points," and select 1601.

- Connect the Agilent N4693-600003 Electronic Calibration Module to the PNA with two
  cables. Proceed to the next Step only after the "READY" signal.

- Choose the menu option 'Calibration' from the main menu bar of the PNA screen,
  In the drop-down menu click on the option 'Calibration wizard'. A dialog box
  called "Calibration wizard: Begin calibration" appears. Click 'next.'

- In the dialog box "Select calibration ports and E-Cal module", verify that the '2 port E-
  Cal' option is selected. Click on 'next'.

- In the dialog box "Electronic calibration step 1 of 1," click on 'measure' and wait until
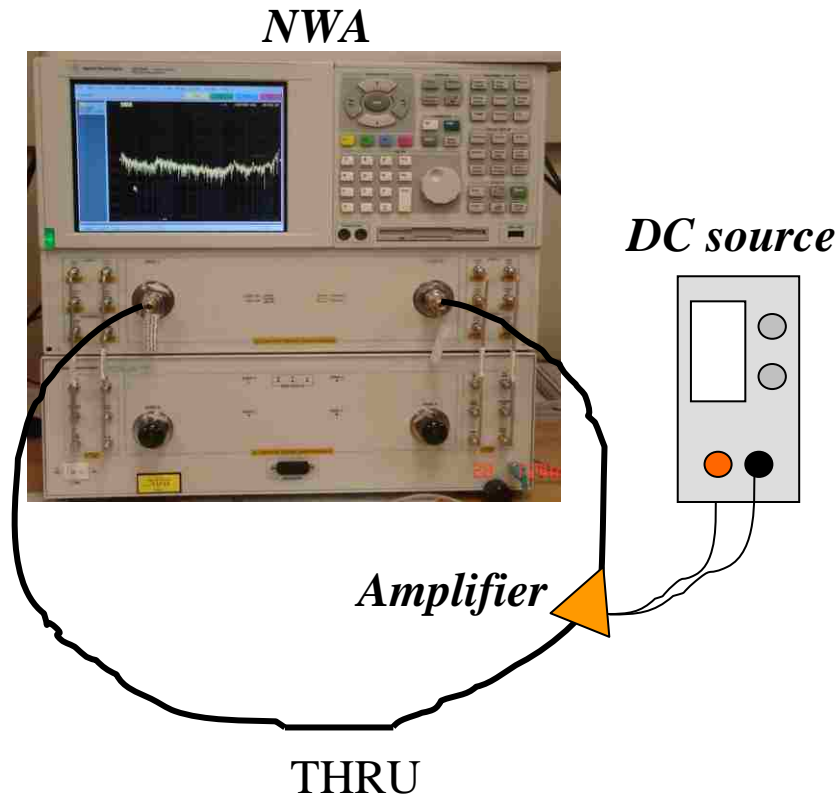 PNA completes calibration.

Figure C.3: THRU Calibration for transfer S-parameter measurement purposes only

- When the "calibration completed in channel 1" dialogue box appears, click "finish". Save the calibration data by clicking 'save as user cal set,' then type the calibration set name. Click 'save.'

- Detach cables from the electronic calibration kit. Connect two Agilent 11901D adapters (Female-Male 2.4-3.5 mm) to the end of the cables.

Frequency Domain Trace Coupling Response

The following explains how to find the characteristic frequency response of the flex-circuit H-field probes so that their frequency range may be observed.
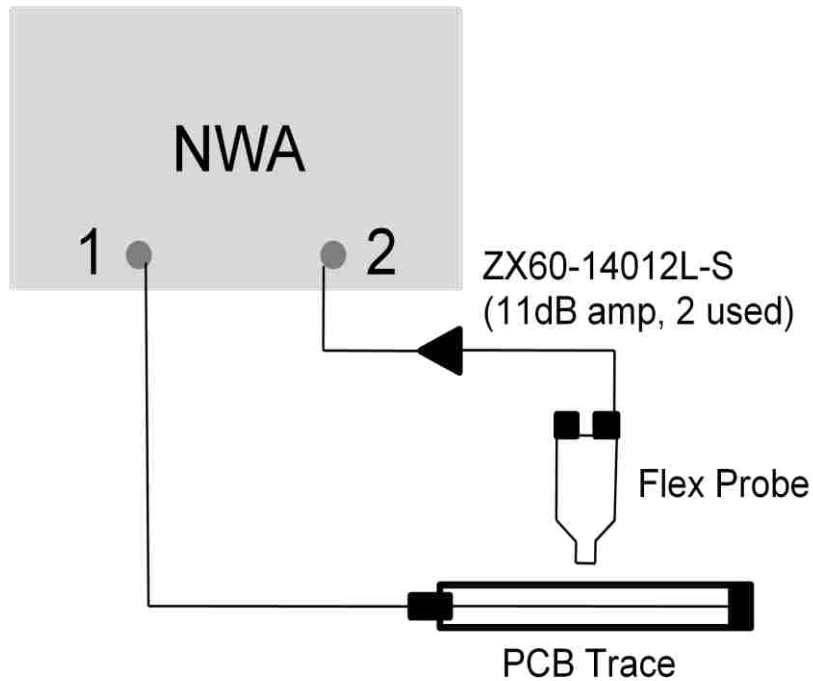
Figure C.4. Setup for frequency domain trace coupling response

Procedure

- Port 1 of the Agilent 50 GHz network analyzer (NWA) is connected to the PCB trace. The other end of the trace is terminated in a matched load.

- Port 2 of the NWA is connected to one end of the differential flex-circuit H-field probe. The other end of probe is terminated in matched 50 Ω loading.

- An amplifier is used to improve the S/N ratio.

- To measure S21 a plot of S21 for the 7×5 mil flex-circuit H-field probe is shown in Figure C.5 below.
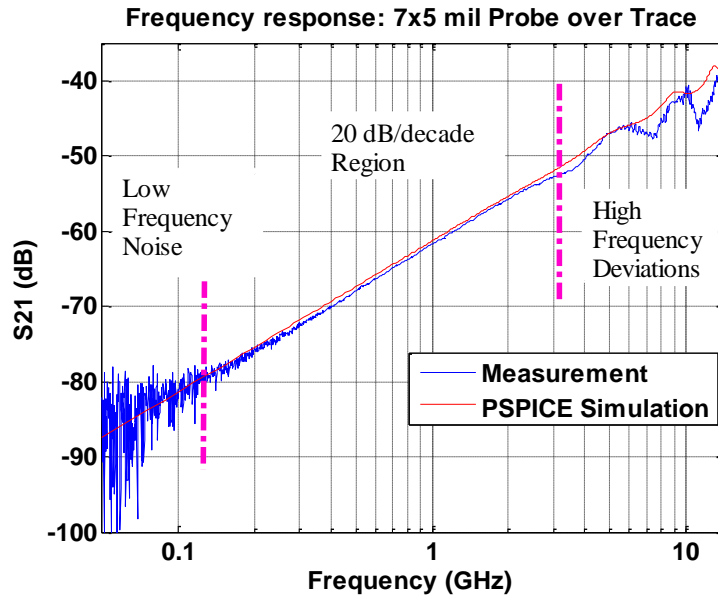
Figure C.5. Frequency response of the 7×5 mil flex probe

Frequency Domain TEM Cell Coupling Response

- The following procedure measures the sensitivity of flex-circuit probes given the fields inside the TEM cell.

- It uses the Crawford TEM cell.

- Calibration for this setup is identical to the calibration procedure described for frequency domain trace coupling response above except that it does not use amplifiers.

- The reference plane is moved to the ends of the cables that will be connected to the TEM Cell, and the flex probe is shown in Figure C.6 below.
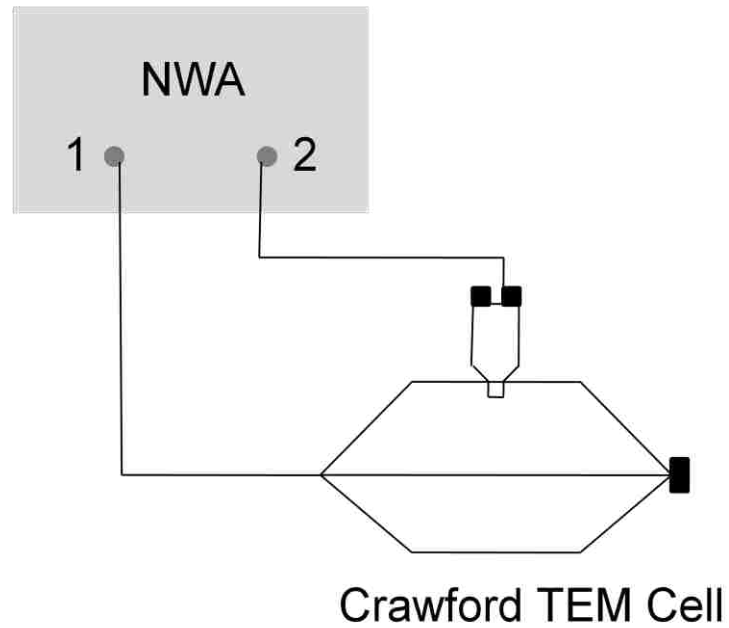
Figure C.6. Setup for frequency domain TEM Cell coupling response

1. Port 1 of Agilent 50 GHz NWA is connected to the TEM Cell.

2. The other end of the TEM cell is terminated in matched load (i.e. 50 Ω).

3. Port 2 of NWA is connected to one end of the differential flex circuit H-field probe. The other end of probe is terminated in matched 50 Ω loading.

4. A slot is milled through a PCB board of size 10×10 mm as shown in figure below which is then placed on the slot on top of the Crawford TEM Cell.

5. Measure |S21|. A plot of S21 for the 7×5 mil flex circuit H-field probe is shown in Figure C 7 below.
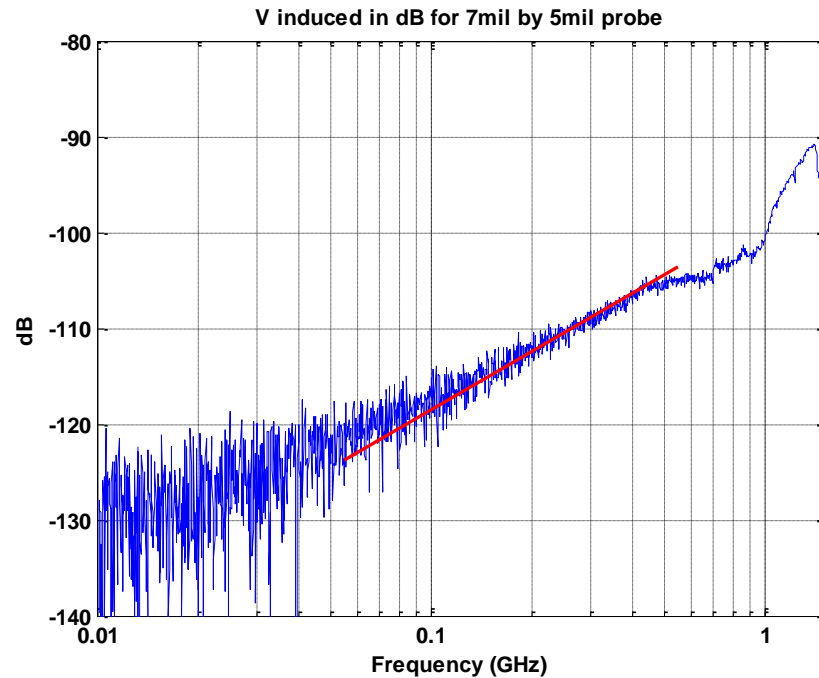
Figure C.7. TEM cell frequency response of the 7×5 mil flex probe

Frequency domain trace coupling response of flex-circuit H-field probe attached to the differential amplifier of the Agilent 1169A active probe

This process measures the frequency domain trace coupling response to determine the flat frequency range.

It uses an Agilent Infinium 54855A. DSO 6GHz 20GSa/s oscilloscope

The network analyzer is an Agilent E5071C 100KHz ~8.5GHz NWA.

A through (THRU) calibration is performed for the two cables attached to the PCB trace beneath the probe and the output of the 1169A active probe.

Instrument settings:

- Swept frequency range: 1MHz to 8GHz.

- IF band: 1 KHz.

- Number of averages: 16.

- Number of points: 1601.

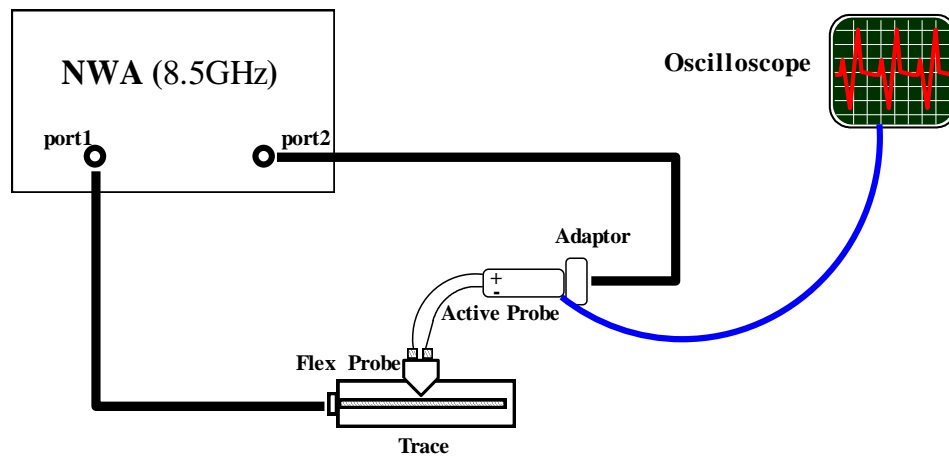- Power level: 10dBm.

Figure C.8. FD trace coupling response of flex probe attached to differential amplifier of

active probe

Procedure:

1. Port 1 of NWA was connected to the PCB trace, which is terminated in a
   matched load on the other end.

2. Port 2 of the NWA was connected to the output of the Agilent 1169A active probe.

3. The probe is powered using the Agilent Infinium 54855A DSO oscilloscope.

4. A special connector was used to connect the oscilloscope, the active probe, and the output of the active probe. This connector was developed in the EMC laboratory Missouri University of Science and Technology by Huang Wei.

5. The differential amplifier of the 1169A active probe was connected to the flex-circuit H-field probe. The probe head on the browser of the 1169A active probe was clipped off and replaced by two SMA connectors, which in turn could be connected to the two ends of the differential flex-circuit H-field probe.

6. The probe was held close to the PCB trace (but not in contact with it) so that the plane of the loop was parallel to the PCB trace beneath it.

7. The transfer parameter |S21| is measured.
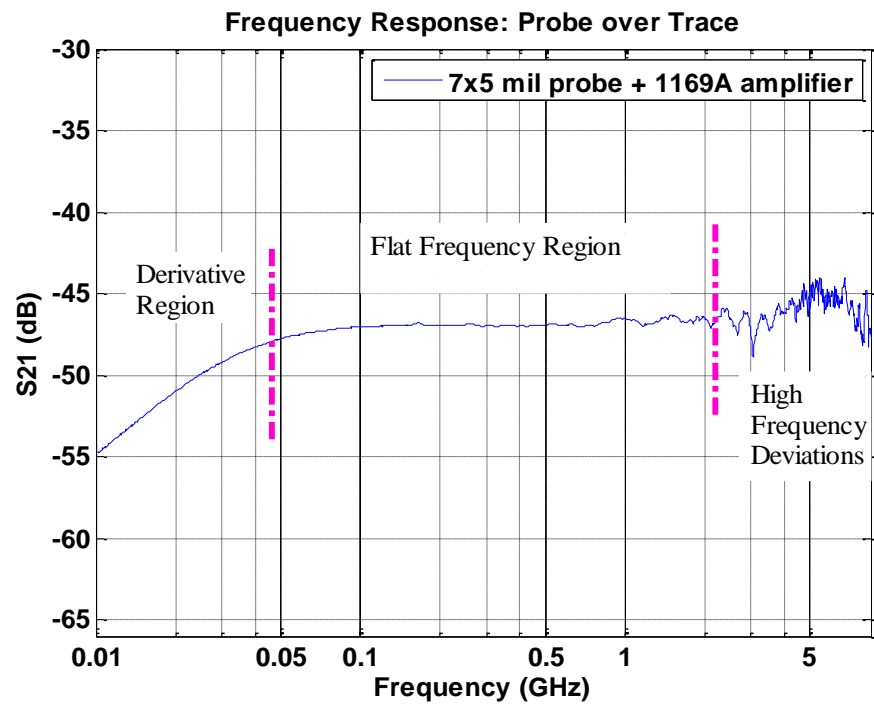
8. Figure C.9 plots the frequency response.

Figure C.9: Frequency response of the flex probe attached to the differential amplifier of

the active probe

Frequency domain TEM cell response of flex-circuit H-field probe attached to the differential amplifier of the Agilent 1169A active probe

The following process measures the sensitivity of the combined flex-circuit H-field probe and the differential amplifier of the Agilent 1169A active probe.

It requires an Agilent Infinium 54855A oscilloscope (DSO   6GHz 20GSa/s).

The network analyzer is an Agilent E5071C 100KHz ~8.5GHz NWA

Calibration: A THRU calibration was performed for the two cables that are attached to the PCB trace beneath the probe and the output of the 1169A active probe.

 Instrument settings:

- Swept frequency range: 1MHz to 8GHz.

- IF band: 1 KHz.

- Number of averages: 16.

- Number of points: 1601.

- Power level: 10dBm.

Measurement Procedure:

1. Port 1 of the NWA is connected to the Crawford TEM cell, which is terminated in a matched load on the other end.

2. Port 2 of the NWA is connected to the output of the Agilent 1169A active probe.

3. The probe is powered using the Agilent Infinium 54855A DSO oscilloscope.

4. The differential amplifier of the 1169A active probe was connected to the flex-circuit H-field probe. The probe head on the browser of the 1169A active probe

was clipped off and replaced by two SMA connectors, which were in-turn connected to the two ends of the differential flex-circuit H-field probe.

5. The probe was placed in the slot milled in a 10 mm^2 PCB board, which was then placed onto the TEM cell.

6. The transfer parameter |S21| was measured. Figure C.10 plots the frequency response.
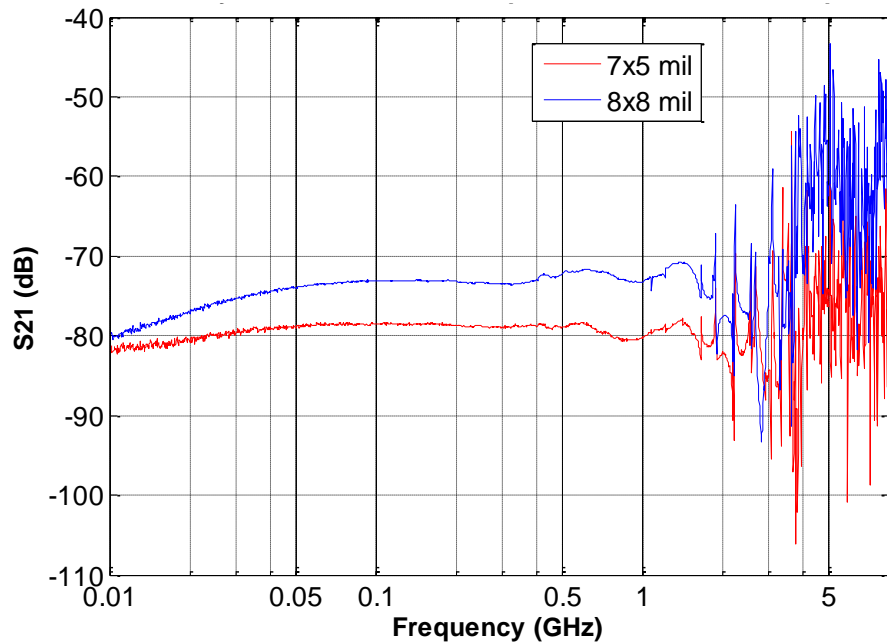

Figure C.10: TEM Cell frequency response of flex circuit H-field probes to measure sensitivity.

Frequency domain Open-strip line cell response of E-field probe based on bow tie antenna design and made with active probe

The following procedure permits evaluation of the frequency response and measurement of the sensitivity of the E-field probe based on a bow tie antenna and using the active probe.

It used an Agilent Infinium 54855A oscilloscope. (DSO   6GHz 20GSa/s)

The network analyzer was an Agilent E5071C 100KHz ~8.5GHz NWA

Calibration: A through (THRU) calibration was performed on the two cables attached to the PCB trace beneath the probe and the output of the 1169A active probe.

Instrument settings:

- Swept frequency range: 1MHz to 8GHz.

- IF band: 1 KHz.

- Number of averages: 16.

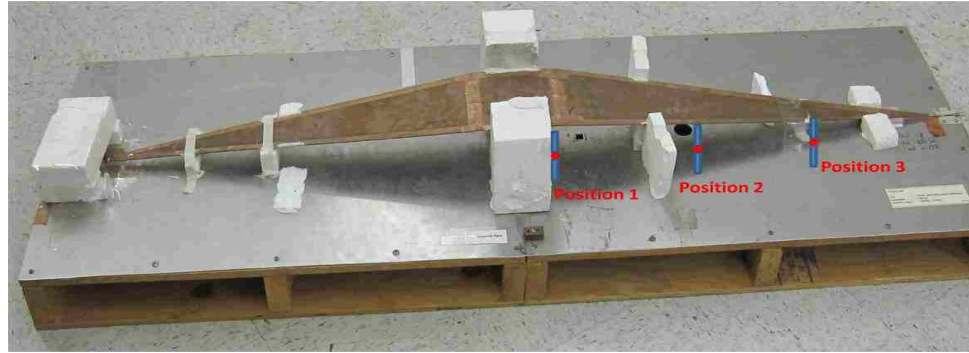- Number of points: 1601.

- Power level: 10dBm.

Figure C.11: Open strip line cell
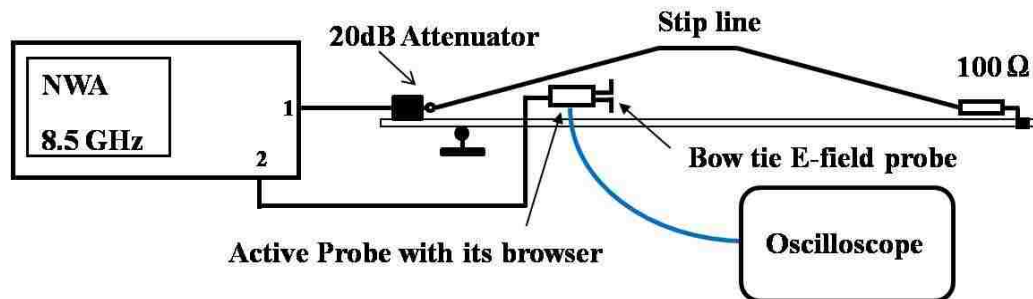
Figure C.12: Schematic of the measurement setup for the E-field probe inside the open

strip line cell.

Measurement Procedure:

1. Port 1 of the NWA was connected to the open strip line cell via a 20 dB attenuator. The attenuator was used to protect the NWA from possible high voltage induced by back coupling. The other end of the open strip line cell was terminated in a matched load, as shown in the figure. The characteristic impedance of the cell was 100 Ω in this case.

2. Port 2 of the NWA was connected to the output of the E-field probe.

3. The probe was powered by an Agilent Infinium 54855A DSO oscilloscope.

4. The design of the E-field probe is discussed in Appendix B.

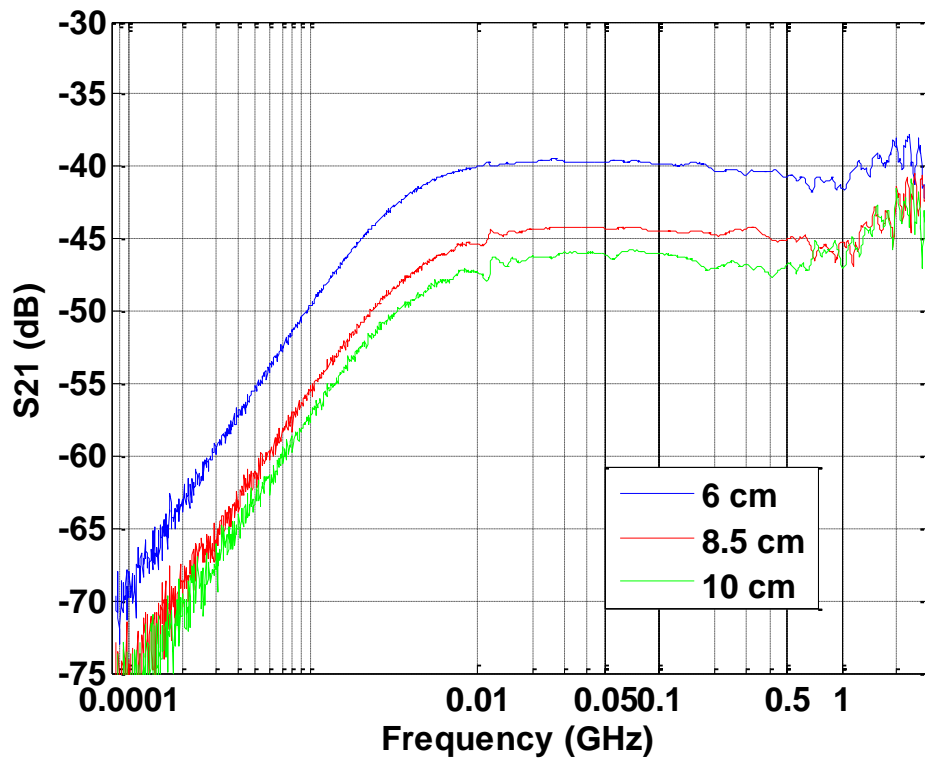5. The transfer parameter |S21| is measured. A plot of the frequency response is shown in the Figure C.13 below.

Figure C.13: Open strip-line cell frequency response of E-field probe at three different

heights inside the cell.

Sensitivity of the E-field probe

The sensitivity of the E-field probe made using the 1169A was found to be 3.3 mV/(V/m).

The two triangular shaped copper tapes are soldered to the tips of the browser of the active probe. This probe is then placed in the TEM Cell which is relatively free of reflections up to 2 GHz. One end of the TEM Cell is connected to Port 1 of the NWA with 20 dB attenuation to avoid ESD damage due to back coupling into the NWA and the E-field probe is connected to Port 2 of the NWA. The S21 measured can be regarded as the output voltage of the probe.

The TEM Cell used has a characteristic impedance of 100 Ω and is terminated on one side in 100 Ω. The reflection coefficient is 1/3 because of the characteristic impedance of TEM Cell being 100 Ω, from equation below:

$$\Gamma = \frac{Z_2 - Z_1}{Z_2 + Z_1} = \frac{V^-}{V^+} \qquad \textbf{(C1)}$$

where Γ is the reflection coefficient; Z_2 and Z_1 are the impedances of the open strip line cell and the NWA; V^- and V^+ are the left going and right going voltage waves.

The output power from the NWA is set as 0 dBm, which is attenuated by 20 dB before appearing at the TEM Cell terminal. Thus, at interface between the TEM cell line and the attenuator, if we look toward the attenuator, we can observe a voltage source with an open voltage of 22.4*2=44.8mV (-20dBm=22.4mVrms) and a 50 ohm resistor. Thus the voltage divided on the TEM Cell is calculated as:

$$V = V_{emf} \square \frac{100}{100 + 50} = V_{emf} \square 2/3 \qquad (C2)$$

where V is the voltage inside the open strip line cell; V_{emf} is the electromotive force voltage of the NWA i.e., the source voltage.

The voltage across the TEM cell is 30 mV.

The electric field inside the Cell at a particular height can be calculated using:

$$V = -\int E \bullet dl$$
(C3)

where V is the voltage induced; E is the electric field; dl stands for the length of an infinitesimal segment of the curve over which the integral of electric field is performed.

The Electric field at the position of the probe where the height of the TEM Cell is 10 cm was found to be 300 mV/m

The S21 of the electric field probe at 10 cm height inside the TEM Cell is -47 dB as shown in Figure C 13. Since the output power of the NWA at port1 is 0dBm, the power measured at port 2 is -47 dBm from:

$$S_{21} = 10 \log\left(\frac{P_2}{P_1}\right)$$
(C4)

where S_{21} is the transfer S-parameter; and P_1 and P_2 are the input and the output power. Since -47 dBm=1 mVrms, we got that the voltage at the port 2 of NWA is 1 mV.

The output voltage of the probe is calculated to be 1 mV. The sensitivity of the electric field probe can be given:

$$Sensitivity = \frac{V_{output of\ probe}}{E_{field\ in\ Volts/meter}}$$
(C5)

The sensitivity of the Electric field probe made using the active probe and the copper tape to form a bow tie antenna was found to be 3.3 mV/(V/m).

APPENDIX D

VALIDATION OF 1-MIL PROBE DESIGN

The following procedure was used to predict the value of |S21| in dB for the 1-mil probe coupled to a microstrip trace.

The trace coupling frequency response of the 7×5 mil flex-circuit H-field probe was a 20 dB/dec curve, as shown in Figure 3-2. This calculation relies on the |S21| in the linear 20 dB/dec region of the curve. The |S21| of the 7×5 mil flex-circuit H-field probe was roughly -85.5 dB at 100 MHz based on both measured and simulated data. The close agreement between simulated and measured results validates the model. Sensitivity can be calculated using equation (4), which is restated below:

$$V_{induced} = A \times \partial B \big/ \partial t$$

The simulation for the 1-mil probe was performed over the same microstrip trace used for the 7×5 mil probe, keeping the solution setup and source settings the same.

The value of |S21| can be expressed as:

$$S21 = 20\log_{10}\left(\frac{V2}{V1}\right) \tag{D1}$$

where V2 is the voltage induced in the probe and V1 represents the source voltage (i.e., excitation voltage on microstrip trace).

For our case of trace coupling response of the probe the V2 represents the voltage induced in the probe and V1 represents the source voltage (excitation voltage on the microstrip trace).

Solving equation 5 yields:

$$\frac{V2}{V1} = 10^{S21/20}$$

$$\frac{V_{7\times5}}{V_{in}} = 10^{\left(S21_{7\times5}/20\right)}$$

$$\frac{V_{1\times1}}{V_{in}} = 10^{\left(S21_{1\times1}/20\right)}$$

$$\frac{V_{7\times5}}{V_{1\times1}} = \frac{10^{\left(S21_{7\times5}/20\right)}}{10^{\left(S21_{1\times1}/20\right)}} = \frac{A_{7\times5}}{A_{1\times1}} = 35$$

The area of the loop of the 7×5 mil flex-circuit H-field probe was 35 mil^2 and that of the 1-mil probe was 1 mil^2.

Hence,

$$S21_{1\times 1} = S21_{7\times 5} - 20\log_{10} 35 = \text{-85.5-30.88} = \text{-116.38 dB} \qquad \text{(D2)}$$
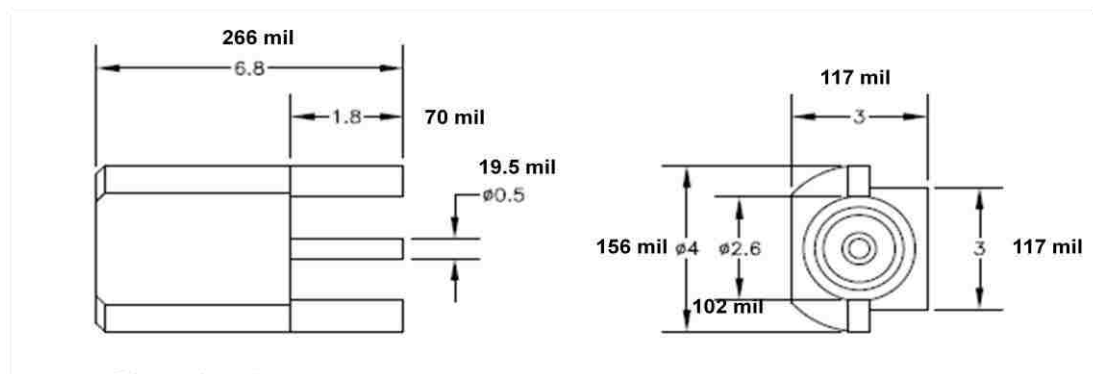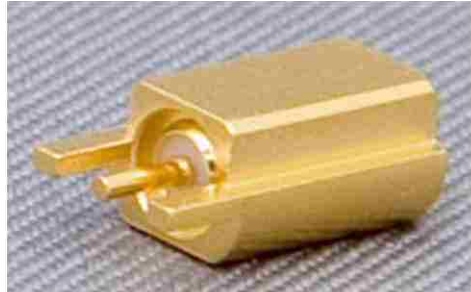
So the expected value of |S21| for the 1-Mil probe at 100 MHz is roughly

-116.38 dB.

APPENDIX E

CONNECTORS

CONNECTORS USED FOR H-FIELD PROBE DEVELOPMENT

The connector mounted on the solder pads of the flex-circuit H-field probes is a mini-SMP. Figure E.1 includes a photograph of the connector.

Figure E.1. Connector test structure

BIBLIOGRAPHY

[1]   IEEE Std 802.3aq, 2006.

[2]   Norman L. Swenson, Paul Voois, Tom Lindsay, Steve Zeng, "Standards compliance testing of optical transmitters using a software-based equalizing reference receiver".

[3]   Ben Willcocks, Nick Weiner, Ian White, Richard Penty, and Jonathan Ingham, "Electronic dispersion compensation steps up to 10-Gbit/s link challenges," CommsDesign, Jan 14, 2004.

[4]   SFF-8431 Specifications for Enhanced 8.5 and 10 Gigabit Small Form Factor Pluggable Module SFP+, Revision 2.2, 19 December 2007.

[5]   A. Ghiasi, "Higher Speed Copper Operation", *IEEE 802.3 HSSG Meeting*, San Francisco, July 17, 2007.

[6]   Vittorio Ricchiuti, Antonio Orlandi, James L. Drewniak, and Francesco De Paulis, "Characterization of serial links at 5.5Gbps on FR4 backplanes", submitted for publication to *EMC Europe,* September 8-12, 2008, Hamburg, Germany.

[7]   William O. Coburn, Calvin Le, David J. De Troye, Gordon E. Blair and Warren Williams, "Electromagnetic Field Measurements Near a Railgun," IEEE transactions on magnetics, Vol 31. No. 1. January 1995

[8]   Farr. E., and Bowen, L.: "A time-domain antenna range – sensors, calibration and signal processing". Book of Abstracts, EURO Electromagnetics' 2000, Edinburg, 30 May – 2 June 2000, p.65

[9]   Tyo, S., and Buchenauer, J., "Compact sensors for time-domain measurements". Book of Abstracts, Euro Electromagnetics '2000, Edinburg, 30 May-2 June 2000, pp.66

[10]   A. Yarovoy, R. de Jongh and L. Ligthart, "Ultra-wideband sensor for electromagnetic field measurements in time domain," IEEE Electronic Letters, Vol.36, No.20

[11]   John P.Casey, "Analysis and Optimization of an Electrically Small Receiving Antenna," IEEE Transactions on EMC, Vol. 33, No. 3, 8/91

[12]   Maria A. Stuchly, "Active Magnetic Field Sensor for Measurement of Transients," IEEE Transactions on EMC, Vol.33, No 4, 11/91

[13]   Masugi, M., Murakawa, K. Kuwabara, N., Ameniya, F., 'Measurement and Analysis of Electromagnetic Pulses caused by Electrostatic Discharge', IEEE Int. Symp. on EMC, 1992, p.361-365

[14]   Carl E. Baum, Edward L. Breen, Joseph C. Giles, John O'Neill, and Gary D. Sower, "Sensors for Electromagnetic Pulse Measurements Both Inside and Away from Nuclear Source Regions," EMC *IEEE transactions.*, Vol. EMC-20, pp. 22-35, Feb. 1978.

[15]   "5968-7141EN data sheet,"1169A 12 GHz InfiniiMax II Series Probe Amplifier, Agilent, USA

VITA

Surbhi Mittal was born on February 27, 1985 in Ambala Cantt, Haryana, India. She completed high school education at Guru Nanak Public School, Sambalpur in 2002. She received the degree of Bachelor of Engineering in Electrical & Electronics Engineering from Manipal Institute of Technology in May 2006. She joined Electromagnetic Compatibility laboratory at Missouri University of Science and Technology (formerly, University of Missouri - Rolla) as a graduate research assistant in August 2007. She received her M.S. degree in Electrical Engineering from Missouri University of Science and Technology in May 2010.